Acta Pharmacologica Sinica (2018) 39: 1421–1438
 1671-4083/18
www.nature.com/aps

Article

Suppression of MIF-induced neuronal apoptosis may underlie the therapeutic effects of effective components of Fufang Danshen in the treatment of Alzheimer's disease

Cheng-jie LIANG[1, 2, #], Jia-huang LI[1, #], Zhen ZHANG[1], Ju-yan ZHANG[1], Shu-qun LIU[3, *], Jie YANG[1, 2, *]

[1]*State Key Laboratory of Pharmaceutical Biotechnology, College of Life Sciences, Nanjing University, Nanjing 210093, China;* [2]*State Key Laboratory of Proteomics, Beijing Proteome Research Center, Beijing Institute of Radiation Medicine, Beijing 100850, China;* [3]*Laboratory for Conservation and Utilization of Bio-resources, Yunnan University, Kunming 650091, China*

Abstract

Fufang Danshen (FFDS or Compound Danshen) consists of three Chinese herbs Danshen (*Salviae miltiorrhizae radix et rhizome*), Sanqi (*Notoginseng radix et rhizome*) and Tianranbingpian (Borneolum, or *D*-borneol), which has been show to significantly improve the function of the nervous system and brain metabolism. In this study we explored the possible mechanisms underlying the therapeutic effects of the combination of the effective components of FFDS (Tan IIA, NG-R1 and Borneol) in the treatment of Alzheimer's disease (AD) based on network pharmacology. We firstly constructed AD-related FFDS component protein interaction networks, and revealed that macrophage migration inhibitory factor (MIF) might regulate neuronal apoptosis through Bad in the progression of AD. Then we investigated the apoptosis-inducing effects of MIF and the impact of the effective components of FFDS in human neuroblastoma SH-SY5Y cells. We observed the characteristics of a "Pendular state" of MIF, where MIF (8 ng/mL) increased the ratio of p-Bad/Bad by activating Akt and the IKKα/β signaling pathway to assure cell survival, whereas MIF (50 ng/mL) up-regulated the expression of Bad to trigger apoptosis of SH-SY5Y cells. MIF displayed neurotoxicity similar to $A\beta_{1\text{-}42}$, which was associated with the MIF-induced increased expression of Bad. Application of the FFDS composite solution significantly decreased the expression levels of Bad, suppressed MIF-induced apoptosis in SH-SY5Y cells. In a *D*-galactose- and $AlCl_3$-induced AD mouse model, administration of the FFDS composite solution significantly improved the learning and memory, as well as neuronal morphology, and decreased the serum levels of INF-γ. Therefore, the FFDS composite solution exerts neuroprotective effects through down-regulating the level of Bad stimulated by MIF.

Keywords: Alzheimer's disease; traditional Chinese medicine; Fufang Danshen; MIF; Bcl-2 family proteins; apoptosis; learning and memory; SH-SY5Y cells; neuroprotection

Acta Pharmacologica Sinica (2018) 39: 1421–1438; doi: 10.1038/aps.2017.210; published online 17 May 2018

Introduction

Alzheimer's disease (AD) is a chronic neurodegenerative disease with the pathological hallmarks of neuritic plaques and neurofibrillary tangles (NFTs) that currently affects over 46.8 million people worldwide[1]. Neuritic plaques are related to the accumulation of the amyloid-beta peptide (Aβ) in brain tissues, while NFTs are associated with cytoskeletal changes that arise from the hyperphosphorylation of microtubule-associated Tau protein in neurons[2]. Aβ peptides are generated by the successive cleavage of APP (amyloid-β precursor protein) by aspartyl proteases (β-secretase or BACE) and a tetramer complex, γ-secretase, which contains presenilins (PS1 and PS2), nicastrin, aph-1 and pen-2[3]. The predominant site of caspase-mediated proteolysis is located in the cytoplasmic tail of APP, and caspase-3 is the predominant caspase involved in APP cleavage[4]. Moreover, APP cleavage occurs in hippocampal neurons *in vivo* following acute excitotoxic or ischemic brain injury, resulting in elevated Aβ peptide formation and neuronal death[4]. Mammalian apoptosis is often regulated by the Bcl-2 family of proteins, the adaptor protein Apaf-1 (apoptotic protease-activating factor 1) and the cysteine protease caspase family[5]. The Bcl-2 family contains both anti-apoptotic and pro-apoptotic proteins. The anti-apoptotic Bcl-2

[#] These authors contributed equally to this work.
[*] To whom correspondence should be addressed.
E-mail yangjie@nju.edu.cn (Jie YANG);
shuqunliu@yun.edu.cn (Shu-qun LIU)
Received 2017-07-17 Accepted 2017-11-26

and Bcl-xL reside in the outer mitochondrial wall and inhibit cytochrome *c* release, whereas the pro-apoptotic Bad and Bax reside in the cytosol but translocate to mitochondria and promote the release of cytochrome *c* following death signaling[6]. Bad translocates to mitochondria and forms a pro-apoptotic complex with Bcl-xL[7], but this translocation is inhibited by survival factors that induce the phosphorylation of Bad, leading to its cytosolic sequestration, which is associated with proximal death and survival signals and results in the activation of pro-apoptotic Bax and Bak or its sequestration by anti-apoptotic Bcl-2 and Bcl-xL[6]. Apaf-1 forms a complex with mitochondrial-released cytochrome *c* and caspase-9 to mediate the activation of pro-caspase-9. Activated caspase-9 in turn cleaves and activates caspase-3 5, 6. Caspases thus appear to play a dual role in the proteolytic processing of APP and the resulting propensity for Aβ peptide formation, as well as in the ultimate apoptotic death of neurons in AD[4].

The currently available therapeutic strategies are mainly targeted at specific symptoms of AD, such as cholinergic activity, neurotrophins, statins, non-steroidal antiinflammatory drugs, hormone replacement therapy, blocking excitotoxicity, Aβ vaccines, immunotherapy, secretase effectors, antioxidants, *etc*[8]. Although Western medicine cholinesterase inhibitors and N-methyl-d-aspartate (NMDA) blockers, such as tacrine, donepezil, rivastigmine, galantamine, and memantine, have been used as the main means to treat AD since 1993, several limitations and even adverse effects, such as stroke, vomiting, diarrhea, and insomnia, exist[9]. Thus, the demand for searching for alternative therapeutic agents from not only synthetic chemicals but also natural plants is increasing. Chinese literature on dementia was first recorded in "Monograph of madness and dementia" of "Jingyue's Complete Works" by Jingyue ZHANG of the Ming dynasty, and traditional Chinese medicine (TCM) has many effective compounds for the treatment of dementia. Prof Fujiwara MICHIHIRO of Fukuoka University of Japan and other researchers have found that Danggui Shaoyao powder and Coptidis decoction for detoxification have good effects in the treatment of AD and vascular dementia (VD). Some Chinese materia medica (CMM), namely *Salvia miltiorrhiza* (Danshen, *Salviae miltiorrhizae radix et rhizome*) (*Latin*, pinyin and pharmacopoeia name in order for each herb), *Polygala tenuifolia* (Yuanzhi, Polygalae radix), *Acorus tatarinowii* (Shichangpu, Acori tatarinowii rhizoma), *Alpinia oxyphylla* (Yizhi, Alpiniae oxyphyllae fructus), and *Uncaria rhynchophylla* (Gouteng, Uncariae ramulus cum uncis), possess acetylcholinesterase inhibitory activities. Fufang Danshen (FFDS or Compound Danshen), which consists of three herbs Danshen (*Salviae miltiorrhizae radix et rhizome*), Sanqi (*Notoginseng radix et rhizome*) and Tianranbingpian (Borneolum, or *D*-borneol), significantly improves the function of the nervous system and brain metabolism, indicating that there may be a new medicinal value of compound Danshen[10]. Notoginsenoside R1 (NG-R1), a novel phytoestrogen isolated from *Panax notoginseng*, can significantly counteract the effects of Aβ by increasing cell viability, reducing oxidative damage (including apoptosis), restoring the mitochondrial membrane potential, and suppressing stress-activated mitogen-activated protein kinase (MAPK) signaling pathways[11]. Tanshinone IIA (Tan IIA), the main active component of *Salvia miltiorrhiza*, may attenuate hypoxia/reoxygenation (H/R)-induced myocardial microvascular endothelial cell apoptosis in rats by inhibiting the JAK2/STAT3 signaling pathway and regulating the expression of p53, Bax, Caspase-3 and Bcl-2, potentially providing a protective effect of Tan IIA[12]. Tan IIA can reduce the risk of AD by inhibiting iNOS, MMP-2 and NF-κB p65 transcription and translation[13]. (+)-Borneol, a monoterpenoid compound, can significantly increase Bcl-2 expression with decreased expression of Bax, protect SH-SY5Y cells against Aβ-induced toxicity, exert an antioxidative effect and suppress apoptosis[14]. Borneol can improve the blood-brain barrier (BBB) distribution of kaempferol[15], while salvianic borneol ester reduces Aβ oligomers and prevents cytotoxicity[16]. Here, we attempted to explore the potential mechanisms by which the FFDS composition may prevent and treat AD.

Furthermore, AD is accompanied by chronic inflammation. Immune modulatory cells, namely, neurogliocytes, release various cytokines including interferon (IFN) and interleukin (IL) and macrophage inflammatory proteins after activation by Aβ accumulation[17]. The excessive secretion of these cytokines then leads to neuronal damage. Specifically, elevated levels of TNF-α and IL-1β are accompanied by activation of Toll-like receptor 4 (TLR4) signaling, while the consequent up-regulation of BACE-1/PS-1 is likely responsible for the accumulation of Aβ, which in turn increases the level of TLR4, thereby creating a positive feedback loop that may constitute the basis for the progression of AD[18]. The macrophage migration inhibitory factor (MIF) is a pro-inflammatory cytokine that promotes the production of several inflammatory mediators such as TNF-α, IL-6 and IFN-γ and, as a pleiotropic cytokine produced mainly by nonneuronal tissue, is involved in the regulation of neuronal functions. Our previous results showed that spinal MIF plays a critical role in the pathogenesis of formalin-induced inflammatory pain by up-regulating the expression of the spinal NMDA receptor subunit NR2B via

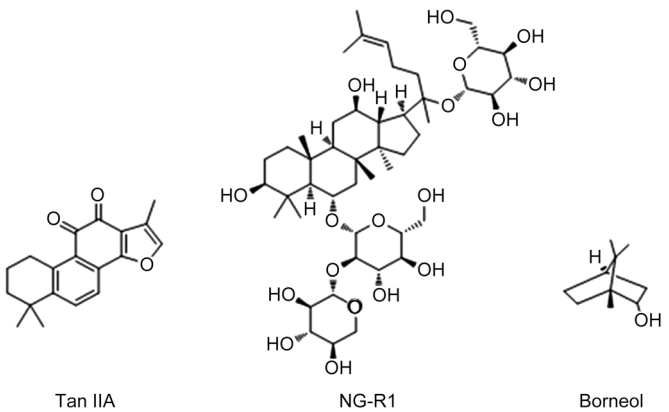

Figure 1. The structures of the components of Fufang Danshen illustrated by ChemDraw v12.0.

the MAPK signaling pathway[19] and contributes to the pathogenesis of neuropathic pain by up-regulation of interleukin-8 and NR2B and the additional production of PGE2 via ERK 1/2 signaling[20]. Importantly, the concentration of MIF is higher in the AD brain than in the healthy brain, indicating that MIF plays a physiological role in the pathogenesis of AD[21].

In addition, network pharmacology, especially TCM network pharmacology, replaces the corollary of rational drug design using "magic bullets", in which multitarget drugs that act on biological networks as "magic shotguns" are identified[22]. Network pharmacology encompasses systems biology, network analysis, connectivity, redundancy and pleiotropy[23] to predict the potential targets of drugs based on public databases or available data from earlier studies and their pharmacological mechanism by using high-throughput technology to analyze the relationship of drugs, proteins and diseases[24]. In this paper, we use network pharmacology to investigate the potential mechanism of action of the components of FFDS, Tan IIA, NG-R1, and borneol, and their combination.

Materials and methods

Computational prediction methods

Databases and software

This paper used the following databases and software: UniProt (http://www.uniprot.org), TTD (http://bidd.nus.edu.sg/group/TTD/ttd.asp), IntAct (http://www.ebi.ac.uk/intact/), PubChem (http://pubchem.ncbi.nlm.nih.gov), PubMed (http://www.ncbi.nlm.nih.gov/pubmed/), KEGG (http://www.KEGG.jp/), Cytoscape, Discovery Studio, and ChemDraw.

Construction of the AD-associated protein-protein interaction network

The protein-protein interaction network and component-protein interaction network were constructed using the software Cytoscape version 2.8.3. These networks were then analyzed using the Analyzer Network plug-in.

AD-related proteins in the TTD database were searched to identify the primary proteins related to AD, and 100 AD-related proteins were selected. Based on the UniProt database (released on March 12, 2015), with "Alzheimer" as the keyword, the proteins that interact with the primary proteins were searched as the secondary proteins in IntAct, and 1133 AD-related proteins were identified. Finally, the AD-related protein–protein interaction network was constructed and displayed in a graphic format using software Cytoscape version 2.8.3. For each of these proteins, we retrieved the PRO IDs from the UniProt database. The two files were further converted into visualized protein networks using the Cytoscape functions "Import->Network from table" where "Source Interaction" and "Target Interaction" corresponded to the 100 primary proteins and the 1133 secondary proteins, respectively. In the networks, each node was a protein entry, and two nodes were connected by an edge if they were related. Entity descriptions and relationship annotations were represented as node or edge attributes. Therefore, the protein-protein interaction network related to Alzheimer's disease (AD-PPIN) was generated. The mean connected degree was given by the "Network Analyzer" of Cytoscape.

Relationship between the components of FFDS and the relevant proteins

The PubMed database (released on Sep 6, 2014) was searched for references related to the components of FFDS, Tan IIA, NG-R1 and (+) borneol, and 23, 20 and 15 proteins relevant to the primary proteins, Tan IIA, NG-R1 and borneol, respectively, were identified. Similarly, the IntAct database was searched for secondary proteins related to the primary proteins, Tan IIA, NG-R1 and borneol. Finally, FFDS component-protein relation networks (FFDS CPRNs) and FFDS component protein-protein interaction networks (FFDS component-related PPINs) were built. The FFDS CPRNs include Tan IIA and its relevant protein (namely, the primary protein) interaction network (Tan IIA-PRN), NG-R1 and its relevant protein interaction network (NG-R1-PRN), and borneol and its relevant protein interaction network (borneol-PRN), while the FFDS component-related PPINs contain the Tan IIA-related PPIN (namely, Tan IIA, its primary protein and secondary protein interaction network), the NG-R1-related PPIN and the borneol-related PPIN. Using Cytoscape's Merge module, the FFDS component-related PPINs (including the Tan IIA-related PPIN, NG-R1-related PPIN and borneol-related PPIN) were integrated and termed the FFDS composition PPIN.

Establishment of the AD-associated FFDS composition-related PPIN

Similarly, the union of the AD-PPIN and FFDS composition PPIN was built using Cytoscape's Merge module. Then, the AD-related FFDS composition PPIN was constructed by combining the AD-PPIN with the FFDS composition PPIN using Cytoscape's Intersection function. The intersection proteins are the likely potential targets for the treatment of AD.

Prediction of the possible AD-related targets of the FFDS components

Based on the AD-related FFDS composition PPIN combined with the Uniprot protein database, PubMed document retrieval and KEGG description of the AD signaling pathway, the possible target proteins of the FFDS components were analyzed, and the mechanism of action of the involvement of the FFDS in AD was further predicted.

Experimental validation methods

Reagents

Medium DMEM/F12, trypsin, trypsin-EDTA (0.25%) and phosphate-buffered solution (PBS) were purchased from Wisent Co, Ltd; fetal bovine serum (FBS) was purchased from Thermo Co, Ltd; DMSO was purchased from Amresco Co, Ltd; penicillin, streptomycin, cell lysis buffer, and Nissl staining were purchased from Beyotime Co, Ltd; MIF was purchased from R&D Systems Co, Ltd; $A\beta_{1\text{-}42}$ and protease inhibitor cocktails were purchased from Sigma Co, Ltd; $AlCl_3$ was

purchased from Nanjing Chemical Reagent Co, Ltd; D-gal was purchased from Biosharp Co, Ltd; Hup A, Tan IIA, NG-R1 and borneol were purchased from Chengdu Herbpurify Co, Ltd; LY294002 was purchased from Selleck Co, Ltd; PS1145 was purchased from Tocris Co, Ltd; ISO-1 and antibodies of Bad, p-Akt, Akt and PI3K were purchased from Abcam Co, Ltd; the p-BAD antibody was purchased from Cell Signaling Technology Co, Ltd.

The MTT kit and BSA were purchased from Biosharp Co, Ltd; the Annexin-FITC/PI Apoptosis Kit was purchased from Vazyme Co, Ltd; the BCA protein assay kit was purchased from Takara Co, Ltd; ELC developing liquid was purchased from Tanon Co, Ltd; PVDF membranes were purchased from Merck Co, Ltd; HRP-linked GAPDH was purchased from Kangchen Co, Ltd; β-Actin and secondary antibodies were purchased from Bioworld Co, Ltd; the INF-γ ELISA Kit and IL-4 ELISA Kit were purchased from MultiSciences Biotech Co, Ltd.

Experimental equipment

The experimental instruments were as follows: Flow cytometer (Accuri C6, BD), Chemiluminescence imaging system (5200, Tanon), CO_2 incubator (MCO-15AC, SANYO), refrigerated centrifuge (5810R, Eppendorf), Safire fluorescent plate reader (TECAN, Durham, NC, USA), Leica microtome (RM2235, Leica, Wetzlar, Germany), Morris water maze (JLBehv-MWMG-1, Shanghai, China) (Prof Zhi-jun ZHANG laboratory, School of Medicine, Southeast University, Nanjing, China), ultrasound (KH-100DE, Kunshan Hechuang Ultrasonic Instrument Co, Ltd, China), *etc*.

Preparation of the $A\beta_{1\text{-}42}$ oligomer

A 4 mmol/L stock solution was prepared by dissolving 0.1 mg $A\beta_{1\text{-}42}$ lyophilized powder into DMSO and then set aside in the fridge at -20 °C until its use.

Then, 5.0 μL $A\beta_{1\text{-}42}$ stock solution was diluted in 35.0 μL 1× PBS to create a 500.0 μmol/L Aβ solution, which was kept at 37 °C for 3 d to allow for $A\beta_{1\text{-}42}$ oligomerization before its use.

To prepare the 4.0 μmol/L Aβ oligomer solution for use, 8.0 μL of the above Aβ oligomer solution was mixed with 1.0 mL cell culture liquid.

MIF solution preparation

Here, 2 μg MIF was dissolved in 0.2 mL sterile 1× PBS containing 0.1% (wt/vol) BSA and mixed evenly to prepare a 10 μg/mL stock solution, which was stored in the fridge at -20 °C.

Then, 5.0 μL of the above MIF solution was blended with 1 mL cell culture liquid to prepare a 50.0 ng/mL MIF solution. A gradient concentration of MIF solutions was then prepared in turn.

Preparation of the solutions containing the effective components of FFDS and their combination

Here, 2.0 mg Tan IIA, 1.0 mg NG-R1 and 10.0 mg borneol were accurately weighed by electronic balance and each added to 2.0 mL 95% ethanol solution. The solutions were ultrasonicated (power 250 W, frequency 33 kHz) for 30 min to thoroughly dissolve the powder, and solutions containing 1 mg/mL Tan IIA, 5.0 mg/mL NG-R1 and 5.0 mg/mL borneol were prepared. Then, 4.0 μL of each of the above solutions were mixed with 1.0 mL medium to prepare working solutions containing 4.0 μg/mL Tan IIA, 20.0 μg/mL NG-R1 and 20.0 μg/mL. The prepared culture medium was filtered through a sterile filter membrane before use.

Similarly, 2.0 mg Tan IIA, 10.0 mg NG-R1 and 10.0 mg borneol were accurately weighed by electronic balance, mixed, and then added to 2.0 mL 95% ethanol solution. The mixture was ultrasonicated (power 250 W, frequency 33 kHz) for 30 min to prepare the FFDS composite solution, containing 1.0 mg/mL Tan IIA, 5.0 mg/mL NG-R1 and 5.0 mg/mL borneol. Then, 4.0 μL of the FFDS composite solution was mixed with 1.0 mL medium to prepare the working FFDS composite solution (including 4.0 μg/mL Tan IIA, 20.0 μg/mL NG-R1 and 20.0 μg/mL borneol in the solution). The prepared culture medium was filtered through a sterile filter membrane before use.

Cell culture and treatments

Human neuroblastoma SH-SY5Y cells were received from Prof Chen-yu ZHANG (School of Life Science, Nanjing University). SH-SY5Y cells were expanded and kept in DMEM/F12 supplemented with 10% FBS and 1% penicillin (100 U/mL)-streptomycin (100 μg/mL) at 37 °C in a 5% CO_2/95% air humidified incubator (MCO-15AC, SANYO). The cells were pretreated with ISO-1 (10.0 μmol/L), LY294002 (10.0 μmol/L) and PS1145 (10.0 μmol/L) for 20 min and then treated with various concentrations of MIF for 36 h. In addition, the cells were pretreated with Tan IIA (4.0 μg/mL), NG-R1 (20.0 μg/mL), and borneol (20.0 μg/mL) for 1 h and then treated with MIF (50.0 ng/mL) for 36 h. Each sample was repeated 5 times. Wells with serum-free medium were used as a negative control.

MTT assay

For the MTT assay, the MTT solution (at a final concentration of 0.5 mg/mL) was added into each well, and cells were incubated at 37 °C for 4 h. The medium was removed, and 150 μL DMSO was added into each well. The plate was gently rotated on an orbital shaker for 10 min to completely dissolve the precipitate. Aliquots (200.0 μL) of the resulting solutions were transferred in 96-well plates, and the absorbance was detected at 570 nm using the microplate spectrophotometer system (Spectra max190-Molecular Devices, Sunnyvale, CA, USA). Cell viability (%) was expressed as a percentage relative to the untreated control group.

Flow cytometry to assess apoptosis

In brief, cells were seeded in 6-well culture plates overnight. At the end of the incubation, cells were digested with 0.25% trypsin for 1 min, and cell culture medium was added to terminate the digestion. The cell suspension was centrifuged at 300×*g* for 5 min at 4 °C. and the supernatant was discarded. Cells were harvested and washed with PBS (10.0 mmol/L phosphate buffer and 140.0 mmol/L saline, pH 7.4),

resuspended in 100.0 μL binding buffer, stained with 5.0 μL annexin V-FITC and 5.0 μL propidium iodide (PI) for 10 min in the dark at 25 °C, and then analyzed by BD Accuri C6 flow cytometry (BD, Biosciences, Franklin Lakes, NJ, USA). Here, the excitation wavelength was 488 nm, and FITC and PI were detected in the FL1 and FL3 channels, respectively. The data were analyzed, and the monochrome scatter diagram was drawn using the BD Accuri CFlow software associated with the Accuri C6 BD flow cytometer.

Western blotting

Similarly, the cell suspension in 6-well plates was collected in a 1.5-mL EP tube and centrifuged at 1000 rounds per minute for 5 min at 4 °C. The supernatant was discarded, and the cells were resuspended in 1.0 mL precooled PBS and centrifuged in the same conditions. The supernatant was discarded, and the cell lysis solution containing 100.0 μL protease inhibitors was added to the cells, which were then placed on ice for 30 min. The cell lysate was centrifuged at 12 000 rounds per minute for 10 min at 4 °C, and the supernatant was retained. The protein concentration was measured with a BCA (bicinchoninic acid assay) protein assay kit (T9300A, Takara).

Approximately 50.0 μg of each protein sample was loaded onto a 10% sodium dodecyl sulfate polyacrylamide gel (SDS-PAGE) and electrophoretically transferred to a polyvinylidene difluoride (PVDF) membrane (Bio-Rad, USA). The membrane was blocked with 5% skimmed milk powder in 1× TBS buffer at 25 °C for 1 h and then incubated with primary antibodies against Bad (1:1000) (Abcam, USA) and β-Actin (1:3000) (Bioworld, USA) at 4 °C overnight. The blots were washed three times for 5 min with Tris-buffered saline Tween-20 and incubated with the secondary horseradish peroxidase (HRP)-conjugated anti-rabbit IgG antibody (1:5000) (Bioworld, USA) at 25 °C for 1 h.

Proteins were visualized using the enhanced chemiluminescence method and visualized on a Tanon-5200 Chemiluminescent Imaging System (Tanon Science & Technology Co, Ltd, Shanghai, China). Finally, the blots were scanned, and densitometric analysis was performed on the scanned images by using ImageJ v4.7 software.

Construction of the $AlCl_3$- and D-gal-induced mouse model and treatment

Male balb/c mice aged 3 weeks (20±2 g) were obtained from the Model Animal Research Center of Nanjing University. Four mice were housed per cage, had free access to food and water and were maintained under constant light (a 12-h light/dark schedule), temperature (22±2 °C) and humidity (65%±5%) conditions.

After 1 week of habituation to the new environment and handling, the animals were randomly assigned to four groups (n=8 in each group): control group, model ($AlCl_3$+D-gal) group, Hup A group, and FFDS composition (TanIIA+NG-R1+borneol) group.

$AlCl_3$ and D-gal were dissolved in sterile saline, whereas Hup A and the FFDS components were dissolved in sterile saline with 2% Tween-20. The mice in the model group, Hup A group and FFDS composition group were intraperitoneally (ip) injected with 1% D-gal (60 mg·kg^{-1}·d^{-1}) and 0.1% $AlCl_3$ (10 mg·kg^{-1}·d^{-1}) for 90 d, whereas the mice in the control group were treated with the same volume of sterile saline.

After 90 d, 0.2 mL 0.5 mg/L Hup A (0.05 mg·kg^{-1}·d^{-1}) was intragastrically (ig) administered to the mice in the Hup A group for 14 d, while 0.2 mL of the FFDS composite solution containing TanIIA (4 mg·kg^{-1}·d^{-1}), NG-R1 (20 mg·kg^{-1}·d^{-1}) and borneol (20 mg·kg^{-1}·d^{-1}) was ig given to the mice in the FFDS composition group for 14 d. The mice in the control group and the model group were treated with the same volume of sterile saline for 14 d.

Animals were treated according to the guidelines of the Regulations of Experimental Animal Administration issued by the State Committee on Science and Technology of China on 14 November 1988. The experiments were carried out under the approval of the Committee of Experimental Animal Administration of Nanjing University. All experiments were conducted in accordance with the standard guidelines for the use and care of laboratory animals, and all surgery was performed under anesthesia. All efforts were made to minimize animal suffering and reduce the number of animals used.

Morris water maze test

The day after the final FFDS composition treatment, the spatial learning and memory of the mice were tested in the Morris water maze as previously described by Vorhees CV and Williams MT[22]. The experimental apparatus consisted of a white circular pool of 100 cm in diameter and 35 cm in height, filled with nontoxic black-dyed water and kept at 23±2 °C. The pool was divided into four quadrants of equal area. A black-colored round platform 4.5 cm in diameter was placed 1 cm below the water surface in a constant position so that it was invisible at water level.

In the place navigation task, four training trials per day were given for five consecutive days in order to train the mice. In each training trial, a mouse was placed into the water maze at one of four determined locations and released, allowing the animal to find the hidden platform. After the mouse found and climbed onto the platform, the trial was stopped, and the escape latency was recorded. Then, the probe trial was conducted on the sixth day. The platform was removed from the pool, and each mouse was allowed to swim freely for 60 s. The time spent in each quadrant was recorded and analyzed. All data (including the escape latency, the time spent in the target quadrant, and the number of times crossing the platform) were monitored and analyzed by a video tracking system (Smart Program, Barcelona, Spain).

ELISA assay

The day after the final FFDS composition treatment, the mice were anesthetized with ether. Blood samples were obtained from mice and centrifuged (12 000 rounds per minute, 10 min) to segregate the serum and then stored at -70 °C until assayed. Serum IL-4 and INF-γ levels were measured using the IL-4

ELISA kit and INF-γ ELISA kit (MultiSciences Biotech Co, Ltd), respectively. This procedure was performed according to the manufacturing protocols and analyzed by the ELISA system. Fluorescence was immediately scanned (t=0 min) using XFluor4 v4.40 software on a Safire fluorescent plate reader (TECAN, Durham, NC, USA).

Nissl staining

After the behavioral tests were completed, the mice were deeply anesthetized with ether and sacrificed by decapitation. Then, their brains were rapidly cleaned with saline over ice and submerged in 4% formaldehyde for pathomorphology by Nissl staining. The whole hippocampus was fixed in 4% paraformaldehyde in 0.01 mol/L PBS (pH 7.4) at 4 °C for 24 h, dehydrated and embedded in paraffin, which was cut into 4–5-μm sections with a microtome (RM2235, Leica, Wetzlar, Germany). The coronal sections were deparaffinized with xylene, serially soaked in anhydrous, 90%, and 70% ethanol, stained with the Nissl staining solution for Nissl bodies according to the manufacturer's instructions (Beyotime Co, Ltd), and again serially soaked in anhydrous, 90%, and 70% ethanol.

The sections were dried, sealed with neutral gum, and then observed under an inverted microscope (CKX41, Olympus) after they were mounted and sealed on slides with neutral balsam. Morphometric analysis of neural cells was performed using an Olympus inverted microscope in the CA1 region of the hippocampus and cerebral cortex. The number of surviving neuronal cells was counted in a 1-mm length of the middle portion of the hippocampal CA1 region and cerebral cortex under ×400 magnification under light microscopy.

Statistical analysis

All data were expressed as the mean±SD. Statistical analysis was performed using the Statistical Analysis System (Graph Pad Prism 5; Graph Pad Software, Inc, San Diego, CA, USA). Group differences in the escape latency during the Morris water maze test were analyzed using two-way analysis of variance (ANOVA). Other data were analyzed by one-way ANOVA for multiple groups and by the Student's *t*-test for two groups. A value of $P<0.05$ was considered statistically significant.

Results

Alzheimer's disease-associated FFDS composition-protein-protein interaction network

The AD-associated protein-protein interaction network (AD-PPIN) contains 1233 nodes (including 100 primary proteins and 1133 secondary proteins) and 1693 edges and has a mean connected degree of 4.363.

On the basis of the FFDS components and their relevant protein relation networks (FFDS CPRNs), the FFDS component protein-protein interaction networks (FFDS component PPINs) were built. The FFDS CPRNs included the Tan IIA-PRN with 26 nodes and 25 edges, the NG-R1-PRN with 21 nodes and 20 edges, and the borneol-PRN with 16 nodes and 15 edges. The FFDS composition PPIN was displayed as a network with 1298 nodes (including Tan IIA, NG-R1, borneol, 49 primary relevant proteins and 1246 secondary interacting proteins), 1912 edges, and a mean connected degree of 2.77. There were 25, 20 and 15 proteins related to Tan IIA, NG-R1 and borneol, respectively, including 9 overlapping proteins (Table 1). Of these 9 overlapping proteins, there were 4 proteins, MAPK14 (p38α MAPK), MAPK1 (p42 MAPK or ERK2), NFKBIA (NFκB inhibitor alpha, IκBα) and MAPK3 (p44 MAPK or ERK1), that were related to both NG-R1 and borneol; 4 proteins, BCL2 (Bcl-2), BAX (Bax or Bcl-2-like protein 4), CASP3 (caspase-3) and CASP9 (caspase-9), that were related to both Tan IIA and NG-R1; and one protein, MAPK8 (c-Jun N-terminal kinase, JNK1), that was related to both Tan IIA and borneol. Moreover, Tan IIA was mainly involved in regulating apoptosis, caspase 9/3, cyclin, microtubules, *etc*. NG-R1 was primarily associated with MAPKs, NF-κB, AP-1, NF-E2 (Nuclear factor erythroid 2), *etc*. Borneol was chiefly related to MAPKs, NFκB, P450, *etc*.

The combination of the AD-PPIN and FFDS component PPINs represents the AD-related FFDS composition protein-protein interaction networks (AD-related FFDS composition PPINs) with 54 nodes (including Tan IIA, NG-R1, borneol, 10 primary proteins and 41 secondary proteins), 130 edges, and a mean connected degree of 4.81 (Figure 2). There were 12 important node proteins identified by having a higher degree than the average degree of 4.81, including the ten primary proteins (*ie*, IKBKB, NFKBIA, CHUK, MAPK1, MAPK8, MAPK14, BCL2, JUN, MAPK9 and AKT1), PPP2CA (serine/threonine-protein phosphatase 2A catalytic subunit alpha isoform), and HSPA9 (Mitochondrial 70-kDa heat shock protein, mtHsp70) (Table 2). The five nodes related to NG-R1 were MAPK14, MAPK1, NFKBIA, BCL2 and JUN (transcription factor AP-1); the 4 nodes related to borneol were MAPK14, MAPK1, NFKBIA and MAPK8; the 6 nodes related to Tan IIA were MAPK8, BCL2, AKT1, CHUK (IKKα), IKBKB (IKKβ) and MAPK9 (JNK2). The following important proteins were also included: ATF2 (activating transcription factor 2), CASP8 (cysteine-aspartic acid protease), IKBKG (NFκB kinase subunit gamma, IKK-γ), RELA (NF-κB p65 subunit), NFKB2 (NF-κB p52 subunit), NFKBIB (NFκB inhibitor beta, IκBβ), MAP3K3 (MAPK kinase 3), ARRB1 (arrestin beta 1), CALM1 (calmodulin 1), CLTC (clathrin heavy chain), TP53 (cellular tumor antigen p53), HSPA8 (heat shock cognate 71-kDa protein or Hsc70 or Hsp73), TUBB (tubulin beta class I), PPP2CB (serine/threonine-protein phosphatase 2B catalytic subunit alpha isoform), APP, BCL2L1 (Bcl-2-like 1 or Bcl-xL and Bcl-xS), and BAD (Bcl-2-associated death promoter or Bad). This observation was supported by a set of 20 candidate genes of kinases involved in tau phosphorylation based on a group of 729 Spanish late-onset AD patients and 670 healthy controls, such as p38α MAPK, JNK1 and 2, ERK2, *etc*[25].

By combining the description of the key nodes in the KEGG database with the function analysis of the key nodes through the literature search, we hypothesized that MIF might regulate apoptosis by regulating the expression level of Bad, which could control the progression of AD through the involvement

Table 1. Compound Danshen components and their related proteins and the degrees of their proteins in the Compound Danshen component related protein-protein interaction networks (FFDS' C-PPINs).

Proteins	Name	Degree			
		Total*	Tan IIA	NG-R1	Borneol
MAPK14	Mitogen-activated protein kinase 14, p38α MAPK	130	0	107	107
HSPA5	78 kDa glucose-regulated protein	124	124	0	0
MAPK1	Mitogen-activated protein kinase 1, p42 MAPK, and ERK2	111	0	86	86
CDK2	Cyclin-dependent kinase 2	106	106	0	0
PARP1	Poly [ADP-ribose] polymerase 1	100	100	0	0
CDK4	Cyclin-dependent kinase 4	90	90	0	0
FOS	Proto-oncogene c-Fos	90	0	90	0
NFKBIA	NF-kappa-B inhibitor alpha, IκBα	88	0	75	75
AKT1	RAC-alpha serine/threonine-protein kinase	79	77	0	0
BCL2	Apoptosis regulator Bcl-2	77	51	51	0
IKBKB	Inhibitor of nuclear factor kappa-B kinase subunit beta, IKKβ	74	72	0	0
JUN	Transcription factor AP-1	72	0	69	0
MAPK3	Mitogen-activated protein kinase 3	71	0	62	62
MAPK8	Mitogen-activated protein kinase 8, JNK1	64	56	0	56
CHUK	Inhibitor of nuclear factor kappa-B kinase subunit alpha, IKKα	62	60	0	0
GFAP	Glial fibrillary acidic protein	57	0	0	57
BAX	Apoptosis regulator BAX	53	35	35	0
CDK5	Cyclin-dependent kinase 5	50	50	0	0
CDKN1B	Cyclin-dependent kinase inhibitor 1B	50	50	0	0
MAPK9	Mitogen-activated protein kinase 9, JNK2	44	43	0	0
KDR	Vascular endothelial growth factor receptor 2	36	0	35	0
MAPT	Microtubule-associated protein tau	35	35	0	0
NOS3	Nitric oxide synthase, endothelial	30	0	30	0
CASP3	Caspase-3	28	24	24	0
PPARG	Peroxisome proliferator-activated receptor gamma	26	26	0	0
CAT	Catalase	25	0	0	25
AKT2	RAC-beta serine/threonine-protein kinase	23	0	23	0
VEGFA	Vascular endothelial growth factor A	21	20	0	0
CASP9	Caspase-9	18	13	13	0
BIRC5	Baculoviral IAP repeat-containing protein 5	15	15	0	0
NFE2	Transcription factor NF-E2 45 kDa subunit	13	0	13	0
PARP4	Poly [ADP-ribose] polymerase 4	13	13	0	0
HMOX1	Heme oxygenase 1	11	0	11	0
TXNIP	Thioredoxin-interacting protein	11	0	11	0
NFE2L2	Nuclear factor erythroid 2-related factor 2	10	0	10	0
ABCB1	Multidrug resistance protein 1	9	0	0	9
ICAM1	Intercellular adhesion molecule 1	8	0	0	8
ABCC1	Multidrug resistance-associated protein 1	8	0	0	8
NOS2	Nitric oxide synthase, inducible	7	0	0	7
KLK3	Prostate-specific antigen	5	5	0	0
PIK3C2A	Phosphatidylinositol 4-phosphate 3-kinase C2 domain-contain-A	4	0	4	0
ANK1	Ankyrin-1	3	0	0	3
AKT3	RAC-gamma serine/threonine-protein kinase	3	0	3	0
EIF4E3	Eukaryotic translation initiation factor 4E type 3	3	3	0	0
DHFRL1	Dihydrofolate reductase, mitochondrial	2	2	0	0
GABRA1	Gamma-aminobutyric acid receptor subunit alpha-1	2	0	0	2
TRPA1	Transient receptor potential cation channel subfamily A member 1	1	0	0	1
CYP2D	Cytochrome P450 2D6	1	0	0	1
PIK3BC	Phosphatidylinositol 4,5-bisphosphate 3-kinase catalytic subunit beta isoform	1	0	1	0

Note: * means FFDS' composition, including Tan IIA, NG-R1 and borneol.

of the MIF-Akt-Bad and MIF-IKK-Bad pathways (Figure 3). Therefore, we further speculated that the combination of the FFDS components may play a therapeutic role in AD through the regulation of Bad.

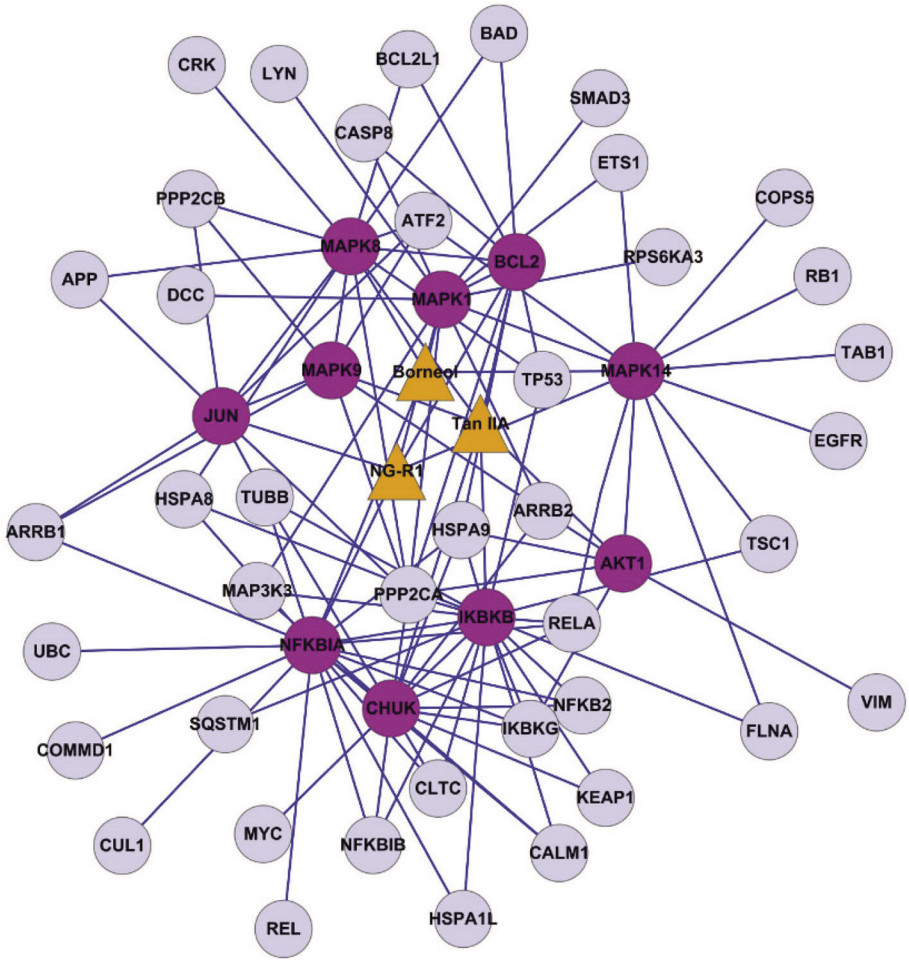

Figure 2. AD-related FFDS composition protein-protein interaction network (PPIN) with 54 nodes, 130 edges and a mean connected degree of 4.81. Here, the FFDS components, their related primary proteins and the secondary interacting proteins are displayed by a yellow triangle, a purple dot and a pink or light blue dot, respectively.

Effects of phosphorylation of Bad on MIF-stimulated SH-SY5Y cells

The MTT assay showed that treatment with ISO-1 (inhibitor of MIF), LY294002 (inhibitor of p-Akt) or PS1145 (inhibitor of p-IKKα/β) for 36 h had no impact on the growth of SH-SY5Y cells (Figure 4A). However, the addition of 8.0 ng/mL MIF to

Table 2. The nodes and the degrees of their proteins in AD related FFDS' composition PPIN.

Name	Degree	Name	Degree	Name	Degree	Name	Degree
IKBKB	20	CASP8	4	APP	2	DCC	1
NFKBIA	19	IKBKG	4	ARRB2	2	EGFR	1
CHUK	15	RELA	4	BAD	2	LYN	1
MAPK1	15	ARRB1	3	BCL2L1	2	MYC	1
MAPK8	14	CALM1	3	CRK	2	RB1	1
MAPK14	13	CLTC	3	ETS1	2	REL	1
BCL2	10	HSPA8	3	FLNA	2	RPS6KA3	1
JUN	10	MAP3K3	3	HSPA1L	2	SMAD3	1
MAPK9	8	NFKBIB	3	KEAP1	2	SQSTM1	1
PPP2CA	8	NFKB2	3	TSC1	2	TAB1	1
AKT1	7	PPP2CB	3	COMMD1	1	UBC	1
HSPA9	5	TP53	3	COPS5	1	VIM	1
ATF2	4	TUBB	3	CUL1	1		

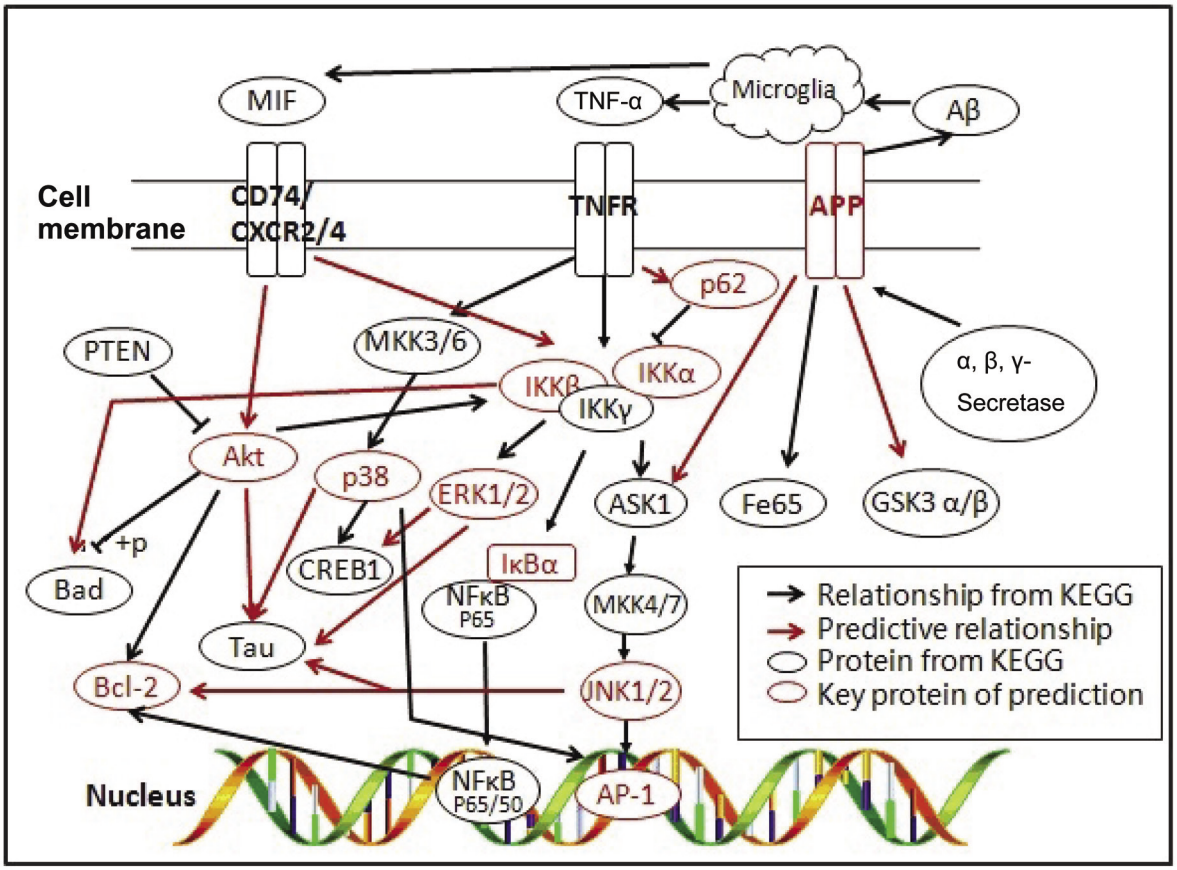

Figure 3. Prediction of the molecular mechanism of the key nodes in the AD-related FFDS C-PPIN through the combination of the description of the key nodes in the KEGG database with the function analysis of the key nodes determined from the literature. The key nodes in AD, which may participate in the signal path diagram, are summarized.

the co-culture for 36 h after ISO-1, LY294002 or PS1145 treatment for 20 min led to a significant decrease in the growth of SH-SY5Y cells in the LY294002-treated group and PS1145-treated group (Figure 4B). The results demonstrated that SH-SY5Y cell growth is inhibited by MIF when the phosphorylation of Akt or IKKα/β was blocked.

Western blotting results showed that after treatment with different concentrations of MIF for 30 min, the expression of p-Bad in SH-SY5Y cells was up-regulated in a dose-dependent manner, and the ratio of p-Bad/Bad was significantly correlated with the MIF dose (Figure 4C). Moreover, MIF induced the phosphorylation of Akt and Bad. However, ISO-1 blocked this phosphorylation, whereas LY294002 and PS1145 only blocked the MIF-induced phosphorylation of Bad (Figure 4D).

Effects of the FFDS components on MIF-induced apoptosis in SH-SY5Y cells

The MTT assay showed that MIF significantly inhibited the growth of SH-SY5Y cells in a dose-dependent manner (Figure 5A), whereas the FFDS components and their combination presented no toxic effects on the growth of SH-SY5Y cells. Tan IIA and the FFDS composition significantly improved the inhibition of SH-SY5Y cells treated with MIF and had significant protective effects on MIF-induced SH-SY5Y cell damage (Figure 5B).

Bad is a pro-apoptotic protein in the organism, and its increase causes cytotoxicity in SH-SY5Y cells. Western blotting analysis further revealed that the expression of the Bad protein was significantly and dose-dependently promoted by MIF (Figure 5C), whereas Tan IIA and NG-R1 as well as the FFDS composition significantly inhibited the MIF-induced expression of Bad in SH-SY5Y cells (Figure 5D). Particularly, MIF at a concentration of 50.0 ng/mL induced a significant increase in the expression of Bad.

Figure 6A displays the results of the annexin V-FITC/PI double staining of SH-SY5Y cells after incubation with oligomeric $A\beta_{1\text{-}42}$ (4.0 μmol/L) or/and MIF (50.0 ng/mL) for 24 h, revealing that MIF and oligomeric $A\beta_{1\text{-}42}$ individually promoted apoptosis of SH-SY5Y cells, and the co-incubation of MIF and oligomeric $A\beta_{1\text{-}42}$ primarily induced the early phase of apoptosis. Flow cytometry further showed that Tan IIA, NG-R1 and the FFDS composition improved the MIF-induced cell damage and protected the cells (Figure 6B).

Effect of the FFDS composition in mice with AD induced by both $AlCl_3$ and D-gal

The Morris water maze test showed that the mean escape

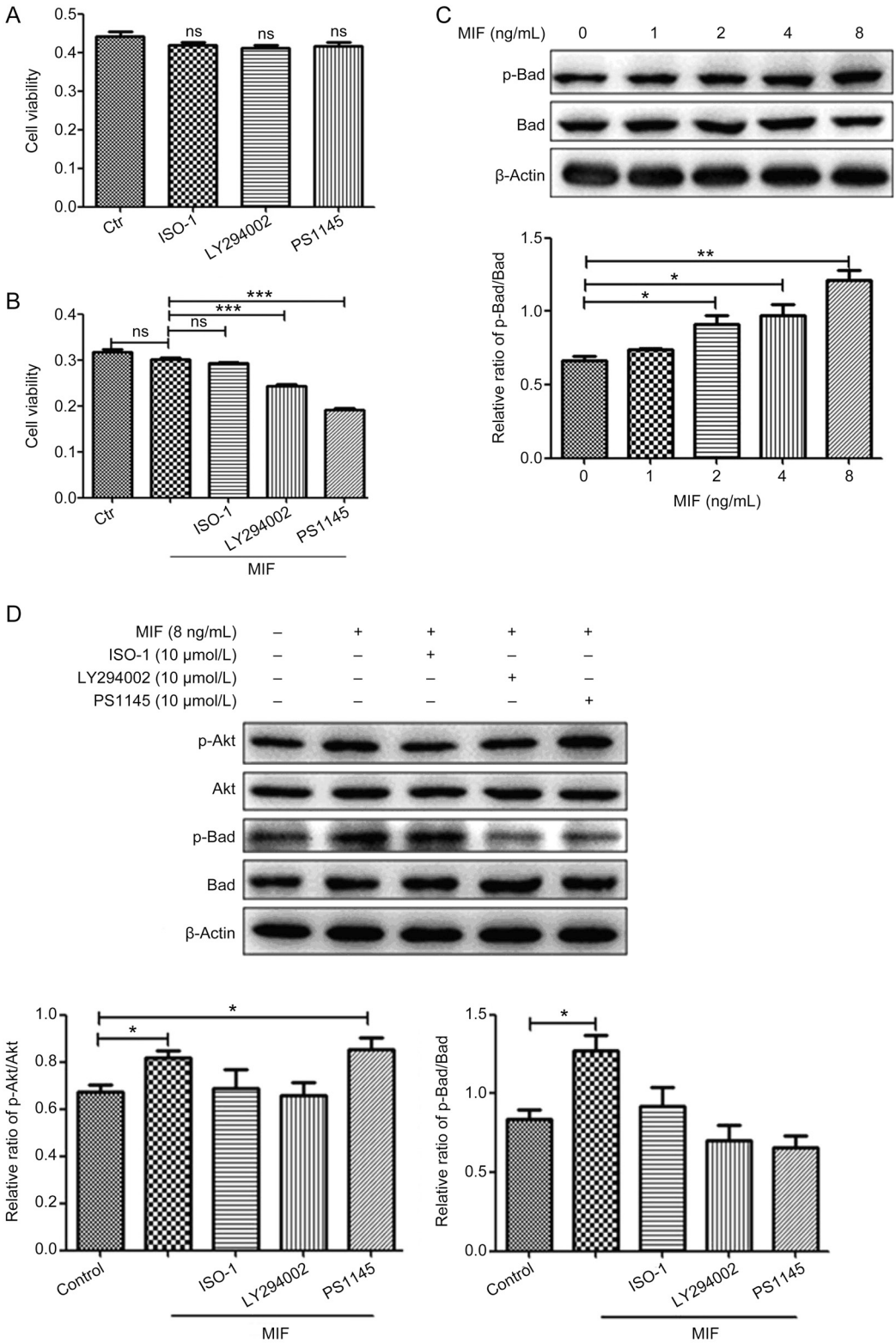

Figure 4. Effects of MIF on the growth of SH-SY5Y cells. (A) SH-SY5Y cells were treated with ISO-1 (10 μmol/L), LY294002 (10 μmol/L) and PS1145 (10 μmol/L) for 36 h, and cell proliferation was examined by MTT assay. (B) SH-SY5Y cells were treated with 8 ng/mL MIF for 36 h after treatment with either ISO-1 (10 μmol/L), LY294002 (10 μmol/L) or PS1145 (10 μmol/L) for 20 min, and cell survival was examined by MTT assay. (C) Effects of MIF on the expression of p-Bad and Bad in SH-SY5Y cells. (D) The expression of Akt, p-Akt, Bad and p-Bad in SH-SY5Y cells after co-culture with some inhibitors (ISO-1, LY294002 and PS1145) and MIF. SH-SY5Y cells were treated with serum starvation for 24 h, and then ISO-1 (10.0 μmol/L), LY294002 (10.0 μmol/L) and PS1145 (10.0 μmol/L) were added to stimulate the cells for 20 min. MIF (8.0 ng/mL) was finally added to the cell co-culture. Data are shown as the mean±SD. $^{*}P<0.05$, $^{**}P<0.01$, $^{***}P<0.001$, ns means no significance.

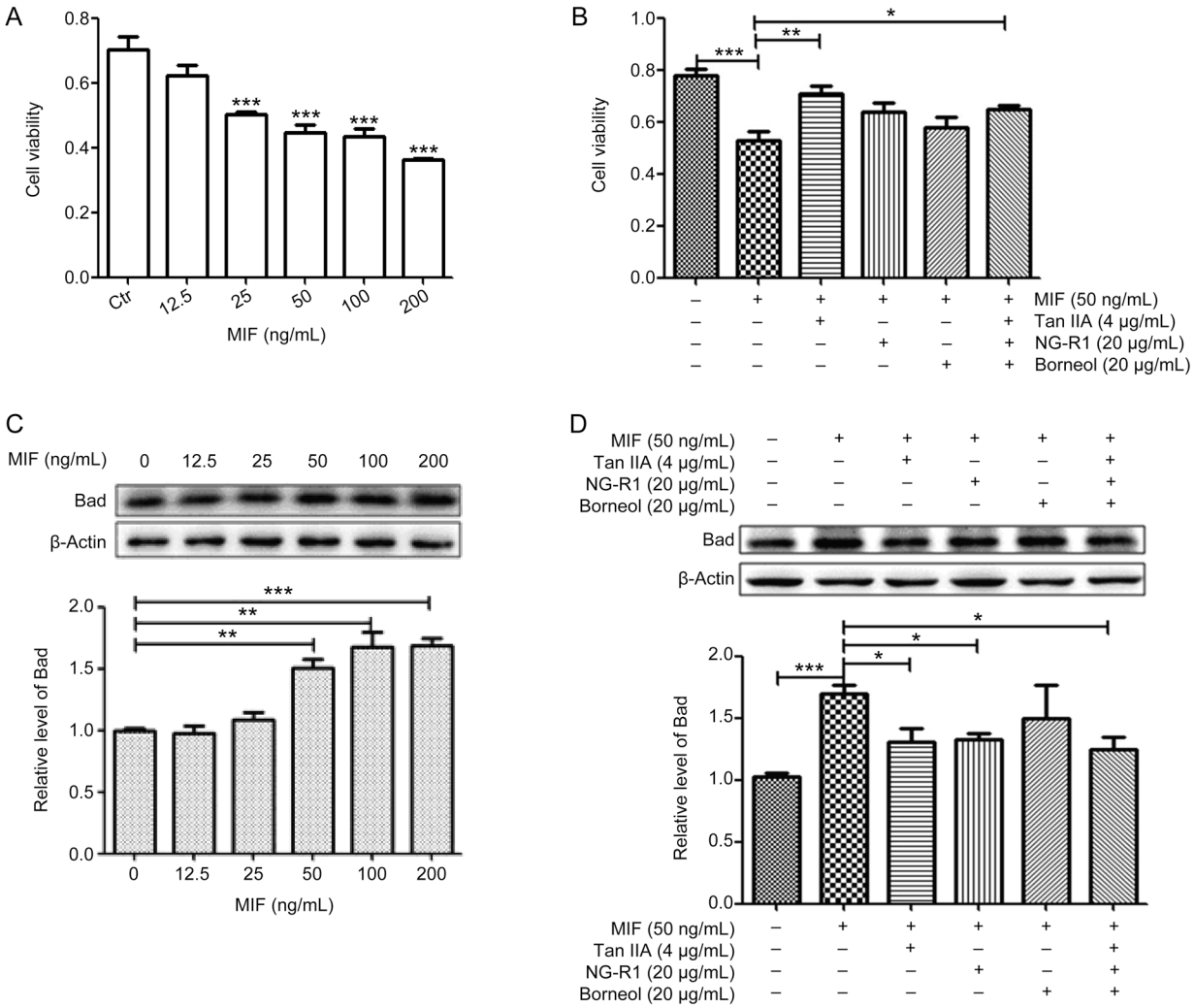

Figure 5. Effect of the FFDS components and their combination on MIF-induced SH-SY5Y cell apoptosis. (A) Effect of MIF on SH-SY5Y cell growth ($^{***}P<0.001$ compared with control). (B) Effect of the FFDS components and their combination on SH-SY5Y cell growth inhibition. (C) Effect of MIF on the expression of Bad in SH-SY5Y cells. (D) Effect of the FFDS components and their combination on the expression of Bad in MIF-induced SH-SY5Y cells. Data are shown as the mean±SD. $^{***}P<0.001$, $^{**}P<0.01$.

latency of mice with AD induced by $AlCl_3$ and D-gal was markedly greater than that of the control group, while the FFDS composition and the Huperzine A (Hup A)-treated groups showed evidence of cognitive repair compared to the model mice in the training periods (Figure 7A). In the probe trial, the platform was removed. The number of platform crossings by the AD mice that were given Hup A or the combination of the FFDS components was slightly higher than that of the AD group (Figure 7B). The AD group spent obviously less time in the target quadrant than the normal group, while the FFDS composition and Hup A groups spent much more time in the target quadrant than the model group (Figure 7C).

ELISA demonstrated that the FFDS composition and Hup A groups exhibited significantly lower concentrations of INF-γ in the serum than the model group, which had increased INF-γ levels (Figure 7D). However, the level of IL4 was unchanged (Figure 7E).

To confirm whether the cortex and hippocampus were damaged by $AlCl_3$ and D-gal toxicity and to estimate the protective effect of the combination of the FFDS components against neuronal impairment, the number of viable surviving neurons was determined by Nissl staining. There were significantly fewer Nissl bodies in the cortex in AD mice than in control mice, whereas treatment with the FFDS composition or Hup A improved this condition, increasing the number of Nissl bodies in the cortex (Figure 8A). The neuronal formation and border in the CA1 area of the hippocampus was diminished in the AD model mice, but the neuronal morphology of the AD mice chronically treated with the FFDS composite solution or Hup A was similar to that of the normal mice in the CA1 (Figure 8B).

Discussion

Analysis of the AD-related FFDS composition PPIN

The FFDS composition could alleviate the AD process through its actions on MAPK, NF-κB, AKT, and JNK signaling path-

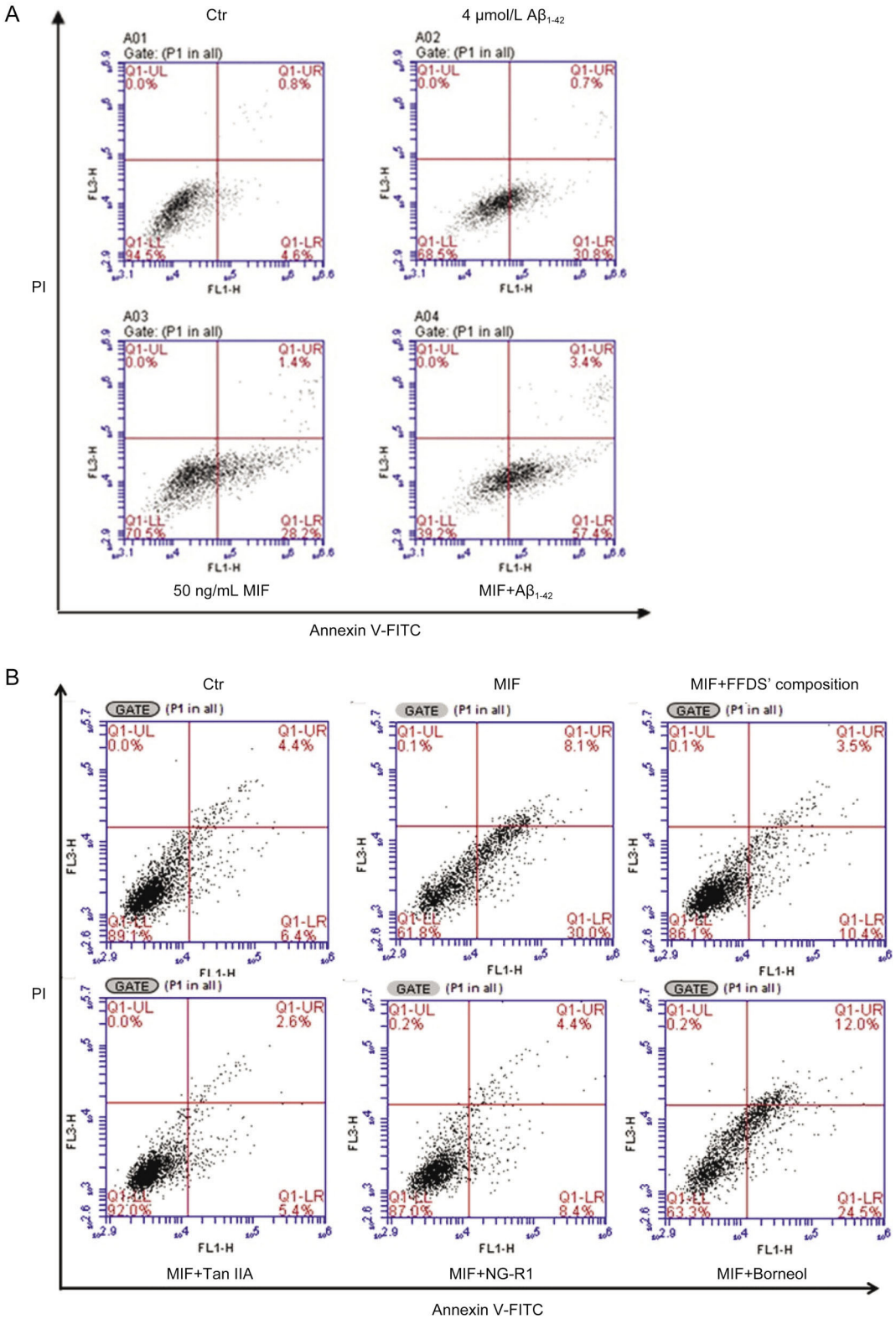

Figure 6. Effect of the FFDS components and their combination on MIF-induced apoptosis in SH-SY5Y cells using flow cytometry. (A) Effect of MIF on SH-SY5Y cells. After SH-SY5Y cells were treated with 50 ng/mL MIF for 24 h, the cell membrane permeability was increased, allowing annexin V to easily cross into the cytoplasm, indicating that the cells were in the early phase of apoptosis and showing similar apoptotic effects as treatment with 4.0 μmol/L $Aβ_{1-42}$. Incubation of SH-SY5Y cells with both MIF and $Aβ_{1-42}$ showed stronger apoptotic effects. (B) Effect of the FFDS components and their combination on MIF-induced apoptosis in SH-SY5Y cells. Here, compound Danshen means the FFDS composition.

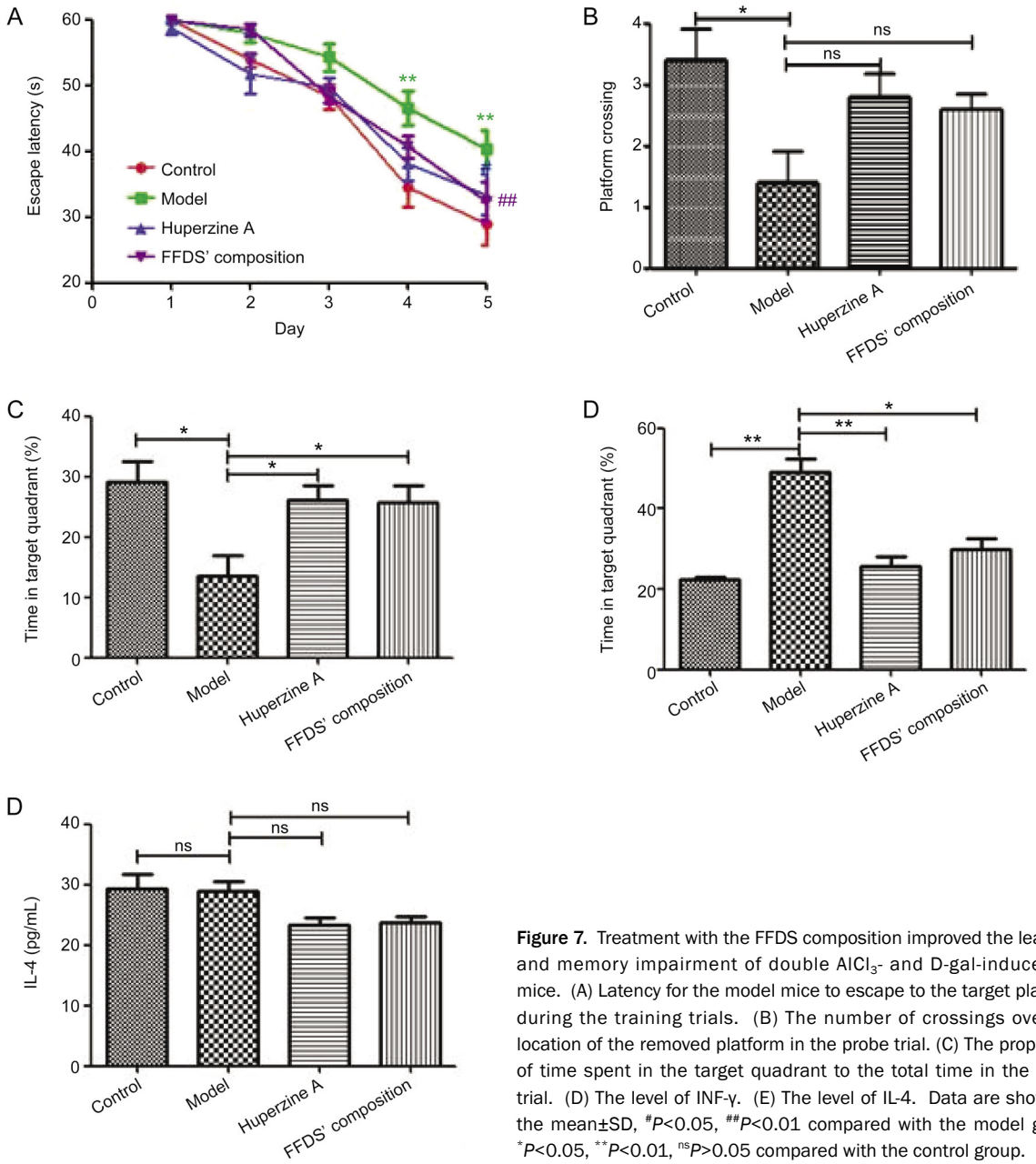

Figure 7. Treatment with the FFDS composition improved the learning and memory impairment of double $AlCl_3$- and D-gal-induced AD mice. (A) Latency for the model mice to escape to the target platform during the training trials. (B) The number of crossings over the location of the removed platform in the probe trial. (C) The proportion of time spent in the target quadrant to the total time in the probe trial. (D) The level of INF-γ. (E) The level of IL-4. Data are shown as the mean±SD, $^{\#}P<0.05$, $^{\#\#}P<0.01$ compared with the model group, $^{*}P<0.05$, $^{**}P<0.01$, $^{ns}P>0.05$ compared with the control group.

ways, as well as through the BCL2-related apoptosis signaling pathway (Figure 3), which was supported by the following reports. The activation of MAPK14 (p38α MAPK) plays a critical role in the regulation of BACE1 degradation, Aβ generation, and the excessive phosphorylation of Tau protein in AD pathogenesis[26], while the β2-adrenergic receptor (β2AR)-protein kinase A (PKA)-JNK pathway mediates Aβ-induced tau pathology by the phosphorylation of tau at Ser-214, Ser-262 and Thr-181 in PS1/APP mice[27]. Activation of the JNK pathway and induction of the AP-1 transcription factor c-Jun are accompanied by neuron death in AD models[28], whereas blockade of JNK-AP1 signaling inhibits Aβ-induced dysregulation of the inflammatory response[29]; therefore, this signaling pathway may serve as a therapeutic target for relieving Aβ-induced neuroinflammation[30]. In addition, the abnormal functioning of the basal forebrain cholinergic neurons and the diminution of ERK2 are critical for the memory disruption associated with AD[31], while phosphorylated MAPK (ERK1, ERK2) expression is associated with early tau deposition in neurons and glial cells in AD, suggesting that activated Ras is the upstream activator of the MEK/ERK pathway of tau phosphorylation in AD[32]. Moreover, hippocampus signal transduction cascades are disrupted in AD as a consequence of the increased $A\beta_{42}$ burden and chronic activation of the ERK MAPK cascade in an alpha7 nicotinic acetylcholine receptor (α7 nAChR)-dependent manner, which eventually leads to the down-regulation of ERK2 MAPK and decreased phosphorylation of cAMP-regulatory element binding (CREB) protein[33].

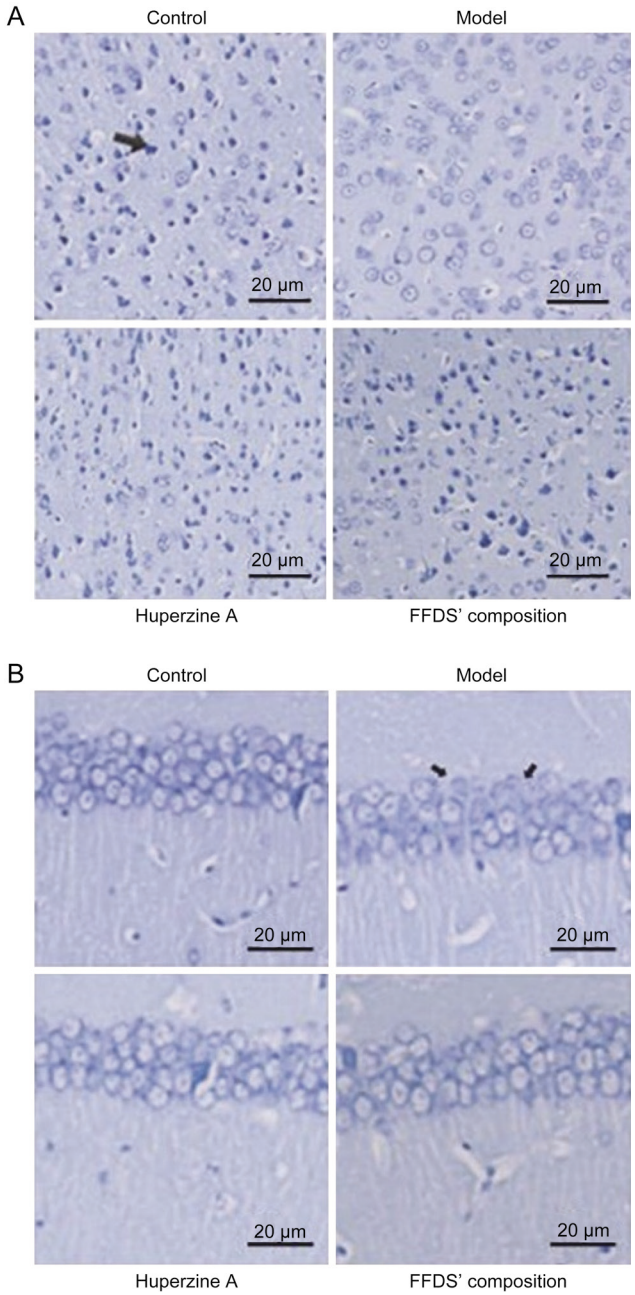

Figure 8. Effect of the FFDS composition on neuronal protection of the cortex (A) and hippocampal CA1 subfield (B) in double $AlCl_3$- and D-gal-induced AD mice. The number of Nissl bodies was counted in a 1-mm length of the middle portion of the hippocampal CA1 region and the cerebral cortex under ×400 magnification using light microscopy.

Additionally, Aβ-induced mitochondrial dysfunction is a hallmark of Aβ-induced neuronal toxicity in AD, thereby decreasing the expression of cytochrome *c* oxidase subunit (COXIII) and inhibiting COX activity via the intramitochondrial IκBα/NF-κB pathway[34]. NF-κB is normally held in an inactive state by the inhibitory proteins IκBs. The IκB kinase complex (IKK) contains two kinase subunits, IKKα and IKKβ, that phosphorylate IκBs at N-terminal sites, resulting in their ubiquitination and degradation in the cytoplasm and allowing NF-κB to go into the nucleus[35]. IKKβ can inhibit TNFα-induced apoptosis through two distinct but cooperative mechanisms: activation of the survival factor NFκB and inactivation of the BH3-only BAD protein, while activated NF-κB further regulates the expression of genes whose products inhibit caspases and prevent prolonged JNK activation[36]. IKKβ deficiency enhanced microglial recruitment to Aβ deposits and facilitated Aβ internalization, perhaps by inhibiting TGF-β-Smad2/3 signaling, but did not affect Aβ production or efflux[37]. In addition, Aβ can trigger microglial activation by interacting with TLR4[38], whereas the TLR4/NF-κB signaling pathway can increase the accumulation of Aβ in lipopolysaccharide (LPS)-treated primary hippocampal neurons of Sprague-Dawley rats and may directly lead to the formation of amyloid plaque in AD[18]. Resveratrol mitigates LPS- and Aβ-mediated microglial inflammation via inhibiting the TLR4/NF-κB/STAT (signal transducer and activator of transcription) signaling cascade[38]. Therefore, inhibition of IKKβ signaling in myeloid cells, especially microglia, improves cognitive function in AD mice by reducing inflammatory activation and enhancing Aβ clearance.

Aβ might induce apoptosis by interacting with neuronal receptors, including the receptor for advanced glycation end-products (RAGE), the p75 neurotrophin receptor (p75(NTR)), and APP[39]. Neurotrophins suppress apoptosis by inducing p75(NTR) polyubiquitination and regulating critical protein kinase cascades 5. Tumor necrosis factor receptor-associated factor 6 (TRAF6) and SQSTM1 (p62) are required for polyubiquitination of p75(NTR), while TRAF6/p62 abrogates the Aβ-mediated inhibition of p75(NTR) polyubiquitination and restores neuronal cell survival. Aβ significantly reduces NF-κB activity by attenuating the interaction of p75(NTR) with IKKβ, whereas p75(NTR) increases NF-κB activity by recruiting TRAF6/p62[39]. Moreover, the disaccharide trehalose is commonly considered to stimulate autophagy by causing a strong accumulation of the autophagic marker proteins LC3-II and p62, altering subcellular trafficking and the metabolism of the AD-associated APP, decreasing the degradation of full-length APP and its C-terminal fragments, and reducing the secretion of the Aβ peptide[40].

Aβ accumulation is responsible for synaptic dysfunction and neuronal cell death. Aβ may down-regulate UCH-L1 (ubiquitin C-terminal hydrolase L1), a deubiquitinating enzyme that functions to regulate cellular ubiquitin, in the AD brain and then compromise synaptic plasticity and neuronal survival[41]. Tau truncation may contribute to synaptic deterioration in AD by aberrant recruitment of parkin and UCH-L1 to mitochondria, making the mitochondria more prone to detrimental autophagic clearance[42]. The Aβ-mediated increase in BACE1 expression through the activation of the JNK-c-jun pathway is accompanied by a decrease in UCH-L1 expression and activity, and the two related events depend on the NF-κB pathway[43]. UCH-L1 could be an attractive target for the development of new therapeutic approaches for AD.

MIF has recently emerged as an important regulator of innate and adaptive immunity. MIF is an upstream activator

of monocytes/macrophages and is centrally involved in the pathogenesis of septic shock, arthritis, and other inflammatory conditions. The MIF-associated ERK 1/2-NMDA receptor or PGE2 cascade accounts for the changes in peripheral nerve injury-induced nociceptive responses[20], where MIF up-regulated the expression of the spinal NMDA receptor subunit NR2B via the MAPK signaling pathway[19]. MicroRNA-608 (miR-608) overexpression inhibited the malignant behavior of glioma stem cells by down-regulating MIF, whereas the inhibition of MIF resulted in the inactivation of the PI3K/AKT and JNK pathways[44]. These observations demonstrate that miR-608 acts as a potential tumor suppressor and provide insight into new therapeutic targets for malignant glioma.

Meanwhile, the function of Bad in the nervous system has recently become a research focus. Phosphorylation of Bad results in its combination with the 14-3-3 protein and a loss of apoptotic activity, whereas dephosphorylated Bad binds with Bcl-xL to dissociate Bax, resulting in an increase in mitochondrial permeability, cytochrome *c* release, and apoptosis of the cell[6]. Bad content in the hippocampal CA1 region of brains stimulated by ischemia was shown to be significantly higher than that in normal brains, and double immunohistochemical staining and Western blot demonstrated that Bad translocated from the cytoplasm to the mitochondria in neurons[45]. Furthermore, piceatannol significantly promoted phosphorylation of Akt and Bad, further suppressed Bcl-2/Bax expression, inhibited cleavage of caspase-9, caspase-3 and PARP, and further showed a comprehensive protective effect against Aβ-induced apoptosis in PC12 cells via the PI3K/Akt/Bad signaling pathway and downstream mitochondria-mediated and caspase-dependent signaling pathway[46].

Therefore, we hypothesized that MIF might regulate apoptosis by regulating the expression level of Bad via the MIF-Akt-Bad and MIF-IKK-Bad pathways (Figure 3), which could control the progression of AD. On this basis, we further speculated that the combination of the effective components of FFDS may play a therapeutic role in AD through the regulation of Bad.

Phosphorylation of Bad in MIF-induced SH-SY5Y cells

MIF is commonly found in the cerebral cortex, hypothalamus, epencephalon and hippocampus. Our study demonstrated that MIF could modulate the growth of SH-SY5Y cells. The MTT assay showed that signal blockers (ISO-1, LY294002 and PS1145) could inhibit the cellular growth. Western blotting showed that MIF could up-regulate the expression of p-Bad in SH-SY5Y cells in a dose-dependent manner, and LY294002 and PS1145 decreased the ratio of p-Bad/Bad. Figure 4 also confirmed that MIF (8.0 ng/mL) up-regulated the expression of p-Bad/Bad by activating Akt and IKKα/β to assure cell survival. However, apoptosis occurred when the signal was blocked. In contrast, MIF (50.0 ng/mL) up-regulated the expression of Bad to trigger apoptosis in SH-SY5Y cells (Figure 5 and 6). As a pleiotropic cytokine, of its many biological activities, the regulatory function of MIF is characterized by a 'Pendular state', showing a significant difference in regulation under different concentrations. For example, the positive and negative regulation of AP-1 is associated with different concentrations of MIF[47]. MIF can modulate the transcriptional activity of the AP-1 gene through its interaction with Jab-1. The expression of p27 is inhibited when the AP-1/c-jun complex binds to AP-1 sites, which is promoted by MIF; however, when the concentration of MIF is excessive, the interaction with Jab-1 is suppressed, and the AP-1/c-jun complex is dissociated. The positive and negative regulation of AP-1 indicates that different concentrations of MIF result in different biological effects. Here, MIF might regulate cellular growth via the MIF-Akt-pBad and MIF-IKK-pBad pathway.

Role of the combination of the effective components of FFDS in MIF-induced apoptosis in SH-SY5Y cells and in $AlCl_3$ and D-gal-induced mice

In SH-SY5Y cells, p38α MAPK has been reported to play a critical role in the regulation of BACE1 degradation and Aβ generation in AD pathogenesis[26]. Previous studies in SH-SY5Y cells have shown that Aβ peptide up-regulated the activity of calcineurin (CaN), consisting of a catalytic subunit (CaN A) and a Ca^{2+}-binding regulatory subunit (CaN B), and increased the cleavage of both calpain I and CaN A[48]. CaN A, a Ca^{2+}/ CALM-dependent protein phosphatase, is activated by proteolytic cleavage of the autoinhibitory domain by calpain I. CaN can mediate Aβ-induced cell apoptosis through the dephosphorylation of Bad and may be the link between Ca^{2+} homeostasis deregulation and apoptotic neuronal death[49]. Aβ and PrP peptides induce CaN overactivation, and, as a consequence, Bad is dephosphorylated and translocated to mitochondria, triggering cytochrome *c* release that may trigger an apoptotic cascade, such as caspase-3 activation. In fact, Bad promotes apoptosis by binding to and inhibiting the actions of the anti-apoptotic proteins Bcl-2 and Bcl-xL, resulting in the activation of pro-apoptotic Bax and Bak. When Bad is phosphorylated in response to survival factors (such as IL-3), it is sequestered in the cytosol, complexed to 14-3-3 proteins, and fails to interact with anti-apoptotic Bcl-2 members, allowing these latter proteins to promote cell survival[6].

MIF may be involved in the neuroinflammation in AD and has been implicated in the toxicity of aggregated Aβ. MIF deficiency is associated with a reduction of astrocyte activation and attenuation of tau hyperphosphorylation in mouse AD models and in Mif (-/-) mice[50]. Therefore, inhibition of MIF and MIF-induced astrocyte activation may be useful in AD prevention and therapy. Here, the MTT assay revealed that MIF (50.0 ng/mL) presented neurotoxicity similar to $A\beta_{1-42}$[51], while Tan IIA and the FFDS composition displayed significant protective effects against MIF-induced SH-SY5Y cell damage. Additionally, MIF as well as $A\beta_{1-42}$ promoted apoptosis of SH-SY5Y cells, whereas Tan IIA, NG-R1 and the combination of the effective components significantly inhibited the SH-SY5Y cell apoptosis induced by MIF. Western Blotting results demonstrated that MIF up-regulated the expression of Bad to trigger apoptosis in SH-SY5Y cells, whereas Tan IIA, NG-R1 and the combination of the effective components sig-

nificantly down-regulated the expression of Bad. Tan IIA protects against cardiac hypertrophy via inhibiting the CaN/NFATc3 pathway[52]; therefore, we speculated that the FFDS composition might play a role in the protection of the nervous system through regulating the level of Bad stimulated by MIF, perhaps via CaN, in AD.

Based on the fact that excessive intake of D-gal can lead to a decrease in the activity of cortical cells, a diminution in the number of hippocampal pyramidal cells, and a deterioration in learning and cognitive abilities, while elevated levels of aluminum in the body can promote Aβ accumulation, an increase in Tau protein content, morphological changes in neurons and a decline in learning and memory function, the senescent mouse model induced by D-gal and $AlCl_3$ is widely used for studying the mechanisms of AD and for drug screening[53], which are believed to be mediated through various mechanisms including apoptosis and oxidative stress[54]. Similarly, the chronic intake of $AlCl_3$ and D-gal can lead to a significant decrease in the spatial learning and memory ability of mice in our experiment. After the AD model mice were treated with the FFDS composition, the escape latency in the water maze was shortened, the number of platform crossings once the platform was removed increased, and the proportion of the time spent in the target quadrant was significantly elevated. The FFDS composite solution was able to improve the intelligence level of the AD model mice and repair the neuronal injury of the mice caused by $AlCl_3$ and D-gal. Just as inflammation accompanies the occurrence and development of AD, the FFDS composite solution was able to relieve the INF-γ level in the mice induced by $AlCl_3$ and D-gal, ease the INF-γ inflammatory reaction, and then alleviate the development of AD. Nissl staining further indicated a reduction in the number of cells in the brains of $AlCl_3$- and D-gal-induced model mice, showing sparse neurons with vacuoles, irregular outlines, and lightly colored cytoplasm. However, these effects were reversed after the mice were treated with the FFDS composite solution, presenting neural cells that were arranged closely, with clear outlines and dark pigmentation. Here, the FFDS composite solution was shown to ameliorate the memory impairment and improve neuronal injury in double $AlCl_3$- and D-gal-induced mice.

Conclusion

TCM compounds are well known to include a complex system of chemicals, in which a group of effective constituents might contribute to the efficacy of a TCM drug. In contrast to Western medicine, the objective of TCM is to improve syndromes of the human body grounded in a concept of wholism and system theory. The combination of specific effective components of a TCM compound, termed a TCM composition, is more competitive in the international market than the TCM compound itself. The former is usually composed of several different components of a TCM compound, similar to Western medicine compounds, whereas the latter is often comprised of different CMMs, having characteristics of multiple components, multiple targets and multiple functions, which is difficult for the international community to recognize due to the diversity and complexity of TCM components and their complex mechanisms. The purpose of this paper was to identify a new FFDS composition for AD therapy and to explore how the effective components of FFDS and their combination play a role in the protection of nerve cells. The AD-related FFDS composition PPIN revealed that the FFDS composition could modulate the expression of Bad via the Akt and/or IKKα/β signaling pathway to protect the brain tissue. Interestingly, characteristics of a "Pendular state" of MIF were observed in our experiments. The regulatory function of MIF is significantly different depending on the MIF concentration. MIF at a concentration of 8.0 ng/mL increased the ratio of p-Bad/Bad by activating Akt and IKKα/β to assure cell survival. In contrast, MIF at a concentration of 50.0 ng/mL up-regulated the expression of Bad to trigger apoptosis in SH-SY5Y cells. Moreover, the FFDS components and their combination did not change the ratio of p-Bad/Bad; however, Tan IIA, NG-R1, and the FFDS composition significantly decreased the expression level of Bad and suppressed MIF-induced apoptosis. Because Tan IIA has been shown to be protective against cardiac hypertrophy via inhibiting the CaN/NFATc3 pathway, we speculated that the FFDS composition might play a role in the protection of the nervous system through regulating the level of Bad stimulated by MIF, perhaps via CaN, in mice with AD induced by long-term intake of $AlCl_3$ and D-gal, not through increasing the ratio of p-Bad/Bad by activating Akt and IKKα/β to assure cell survival similar to piceatannol. Our research has confirmed the protective effects of the FFDS composition on hippocampal neurons in mice with AD induced by $AlCl_3$ and D-gal and determined that the FFDS composition can significantly decrease the serum levels of INF-γ, relieve the inflammation reaction related to INF-γ, and repair the learning and memory impairment of AD mice caused by long-term intake of $AlCl_3$ and D-gal.

Abbreviations

FFDS, Fufang Danshen; AD, Alzheimer's disease; VD, vascular dementia; CaN, calcineurin; Aβ, amyloid-beta peptide; NFTs, neurofibrillary tangles; APP, amyloid-β precursor protein; D-gal, *D*-galactose; $AlCl_3$, aluminum chloride; MIF, macrophage migration inhibitosry factor; NMDA, *N*-methyl-*D*-aspartate; TCM, traditional Chinese medicine; CMM, Chinese materia medica; NG-R1, Notoginsenoside R1; Tan IIA, Tanshinone IIA; Hup A, Huperzine A; H/R, hypoxia/reoxygenation; BBB, blood-brain barrier; IFN, interferon; IL, interleukin; TLR4, Toll-like receptor 4; MIF, macrophage migration inhibitory factor; Apaf-1, apoptotic protease-activating factor 1; DS, Discovery Studio; ADMET, absorption, distribution, metabolism, excretion, and toxicity; PSA, polar surface area; Alog P98, the lipid/water partition coefficient; HIA, human intestinal absorption; PPIN, protein-protein interaction network; PRN, protein relation network; MAPK, mitogen-activated protein kinase; MAP3K3, MAPK kinase kinase 3; NFKBIA, NF-kappa-B inhibitor alpha; JNK, c-Jun N-terminal kinase; NF-E2, nuclear factor erythroid 2; PPP2CA, serine/

threonine-protein phosphatase 2A catalytic subunit alpha isoform; CASP, cysteine-aspartic acid protease; ATF2, activating transcription factor 2; IKBKG, nuclear factor kappa-B kinase subunit gamma; RELA, NF-κB p65 subunit; NFKB2, NF-κB p52 subunit; NFKBIB, NF-κB inhibitor beta, IκBβ; IKK, IκB kinase complex; ARRB1, arrestin beta 1; CALM1, calmodulin 1; CLTC, clathrin heavy chain; TP53, cellular tumor antigen p53; HSPA8, heat shock cognate 71-kDa protein or Hsc70 or Hsp73; TUBB, tubulin beta class I; PPP2CB, Serine/threonine-protein phosphatase 2B catalytic subunit alpha isoform; BCL2L1, Bcl-2-like 1; BAD, Bcl-2-associated death promoter or Bad; β2AR, β2-adrenergic receptor; PKA, protein kinase A; nAChRs, nicotinic acetylcholine receptors; CREB, cAMP-regulatory element binding; COXIII, cytochrome *c* oxidase subunit; LPS, lipopolysaccharide; STAT, signal transducer and activator of transcription; RAGE, the receptor for advanced glycation endproducts; p75(NTR), the p75 neurotrophin receptor; NGF, nerve growth factor; TRAF6, tumor necrosis factor receptor-associated factor 6; ROS, reactive oxygen species; GSK-3β, glycogen synthase kinase-3β; PP2A, protein phosphatase 2A; miR-608, microRNA-608; PBS, phosphate-buffered solution; FBS, fetal bovine serum; BSA, bovine serum albumin; MTT, dimethylthiazol-2-yl-2,5-diphenyltetrazolium bromide; SDS-PAGE, sodium dodecyl sulfate polyacrylamide gels; HRP, horseradish peroxidase.

Acknowledgements

This work was supported by a grant from the Specialized Research Fund for the Doctoral Program of Higher Education of China (20120091110038), the National Natural Science Foundation of China (J1103512 and J1210026), the Open Project of State Key Laboratory of Proteomics (SKLP-O201415), and the Open Project of State Key Laboratory of Pharmaceutical Biotechnology (KF-GN-201405).

Author contribution

Jie YANG designed the study; Chen-jie LIANG, Jia-huang LI, Zhen ZHANG, and Ju-yan ZHANG conducted the experiments; Chen-jie LIANG and Ju-yan ZHANG performed the analysis and the construction of the network pharmacology; Chen-jie LIANG, Jia-huang LI and Zhen ZHANG performed the *in vitro* and *in vivo* experiments; Chen-jie LIANG, Shu-qun LIU, and Jie YANG analyzed the data; and Chen-jie LIANG and Jie YANG wrote the paper.

References

1 Fang J, Wang L, Wu T, Yang C, Gao L, Cai H, *et al*. Network pharmacology-based study on the mechanism of action for herbal medicines in Alzheimer treatment. J Ethnopharmacol 2017; 196: 281–92.
2 De-Paula VJ, Radanovic M, Diniz BS, Forlenza OV. Alzheimer's disease. Subcell Biochem 2012; 65: 329–52 .
3 Marks N, Berg MJ. BACE and gamma-secretase characterization and their sorting as therapeutic targets to reduce amyloidogenesis. Neurochem Res 2010; 35: 181–210.
4 Gervais FG, Xu D, Robertson GS, Vaillancourt JP, Zhu Y, Huang J, *et al*. Involvement of caspases in proteolytic cleavage of Alzheimer's amyloid-beta precursor protein and amyloidogenic A beta peptide formation. Cell 1999; 97: 395–406.
5 Yuan J, Yankner BA. Apoptosis in the nervous system. Nature 2000; 407: 802–9.
6 Yang J, Li JH, Wang J, Zhang CY. Molecular modeling of BAD complex resided in a mitochondrion integrating glycolysis and apoptosis. J Theor Biol 2010; 266: 231–41.
7 Chong ZZ, Maiese K. Targeting WNT, protein kinase B, and mitochondrial membrane integrity to foster cellular survival in the nervous system. Histol Histopathol 2004; 19: 495–504.
8 Castellani RJ, Rolston RK, Smith MA. Alzheimer disease. Dis Mon 2010; 56: 484–546.
9 Zhang Y, Pi Z, Song F, Liu Z. Ginsenosides attenuate d-galactose- and $AlCl_3$-inducedspatial memory impairment by restoring the dysfunction of the neurotransmitter systems in the rat model of Alzheimer's disease. J Ethnopharmacol 2016; 194: 188–95.
10 Liu M, Guo H, Li C, Wang D, Wu J, Wang C, *et al*. Cognitive improvement of compound danshen in an $A\beta_{25\text{-}35}$ peptide-induced rat model of Alzheimer's disease. BMC Complement Altern Med 2015; 15: 382.
11 Ma B, Meng X, Wang J, Sun J, Ren X, Qin M, *et al*. Notoginsenoside R1 attenuates amyloid-β-induced damage in neurons by inhibiting reactive oxygen species and modulating MAPK activation. Int Immunopharmacol 2014; 22: 151–9.
12 Cui ZT, Liu JP, Wei WL. The effects of tanshinone IIA on hypoxia/reoxygenation-induced myocardial microvascular endothelial cell apoptosis in rats via the JAK2/STAT3 signaling pathway. Biomed Pharmacother 2016; 83: 1116–26.
13 Jiang P, Li C, Xiang Z, Jiao B. Tanshinone IIA reduces the risk of Alzheimer's disease by inhibiting iNOS, MMP-2 and NF-κB p65 transcription and translation in the temporal lobes of rat models of Alzheimer's disease. Mol Med Rep 2014; 10: 689–94.
14 Hur J, Pak SC, Koo BS, Jeon S. Borneol alleviates oxidative stress via upregulation of Nrf2 and Bcl-2 in SH-SY5Y cells. Pharm Biol 2013; 51: 30–5.
15 Zhang Q, Wu D, Wu J, Ou Y, Mu C, Han B, *et al*. Improved blood-brain barrier distribution: effect of borneol on the brain pharmacokinetics of kaempferol in rats by *in vivo* microdialysis sampling. J Ethnopharmacol 2015; 162: 270–7.
16 Han M, Liu Y, Zhang B, Qiao J, Lu W, Zhu Y, *et al*. Salvianic borneol ester reduces β-amyloid oligomers and prevents cytotoxicity. Pharm Biol 2011; 49: 1008–13.
17 Akiyama H, Barger S, Barnum S, Bradt B, Bauer J, Cole GM, *et al*. Inflammation and Alzheimer's disease. Neurobiol Aging 2000; 21: 383–421.
18 Wu D, Zhang X, Zhao M, Zhou AL. The role of the TLR4/NF-κB signaling pathway in Aβ accumulation in primary hippocampal neurons. Acta Physiol Sin 2015; 67: 319–28.
19 Wang F, Shen X, Guo X, Peng Y, Liu Y, Xu S, *et al*. Spinal macrophage migration inhibitory factor contributes to the pathogenesis of inflammatory hyperalgesia in rats. Pain 2010; 148: 275–83.
20 Wang F, Xu S, Shen X, Guo X, Peng Y, Yang J. Spinal macrophage migration inhibitory factor is a major contributor to rodent neuropathic pain-like hypersensitivity. Anesthesiology 2011; 114: 643–59.
21 Bacher M, Deuster O, Aljabari B, Egensperger R, Neff F, Jessen F, *et al*. The role of macrophage migration inhibitory factor in Alzheimer's disease. Mol Med 2010; 16: 116–21.
22 Qi Q, Li R, Li HY, Cao YB, Bai M, Fan XJ, *et al*. Identification of the anti-tumor activity and mechanisms of nuciferine through a network pharmacology approach. Acta Pharmacol Sin 2016; 37: 963–72.
23 Zhao N, Li J, Li L, Niu XY, Jiang M, He XJ, *et al*. Molecular network-

based analysis of guizhi-shaoyao-zhimu decoction, a TCM herbal formula, for treatment of diabetic peripheral neuropathy. Acta Pharmacol Sin 2015; 36: 716–23.

24 Goh KI, Cusick ME, Valle D, Childs B, Vidal M, Barabási AL. The human disease network. Proc Natl Acad Sci U S A 2007; 104: 8685–90.

25 Vázquez-Higuera JL, Mateo I, Sánchez-Juan P, Rodríguez-Rodríguez E, Pozueta A, Calero M, *et al*. Genetic variation in the tau kinases pathway may modify the risk and age at onset of Alzheimer's disease. J Alzheimers Dis 2011; 27: 291–7.

26 Schnöder L, Mateo I, Sánchez-Juan P, Rodríguez-Rodríguez E, Pozueta A, Calero M, *et al*. Deficiency of neuronal p38α-MAPK attenuates amyloid pathology in Alzheimer's mouse and cell models through facilitating lysosomal degradation of BACE1. J Biol Chem 2016; 291: 2067–79.

27 Wang D, Fu Q, Zhou Y, Xu B, Shi Q, Igwe B, *et al*. β2 adrenergic receptor, protein kinase A (PKA) and c-Jun N-terminal kinase (JNK) signaling pathways mediate tau pathology in Alzheimer disease models. J Biol Chem 2013; 288: 10298–307.

28 Akhter R, Sanphui P, Das H, Saha P, Biswas SC. The regulation of p53 up-regulated modulator of apoptosis by JNK/c-Jun pathway in β-amyloid-induced neuron death. J Neurochem 2015; 134: 1091–103.

29 Bamji-Mirza M, Callaghan D, Najem D, Shen S, Hasim MS, Yang Z, *et al*. Stimulation of insulin signaling and inhibition of JNK-AP1 activation protect cells from amyloid-β-induced signaling dysregulation and inflammatory response. J Alzheimers Dis 2014; 40: 105–22.

30 Vukic V, Callaghan D, Walker D, Lue LF, Liu QY, Couraud PO, *et al.* Expression of inflammatory genes induced by beta-amyloid peptides in human brain endothelial cells and in Alzheimer's brain is mediated by the JNK-AP1 signaling pathway. Neurobiol Dis 2009; 34: 95–106.

31 Giovannini MG, Cerbai F, Bellucci A, Melani C, Grossi C, Bartolozzi C, *et al*. Differential activation of mitogen-activated protein kinase signalling pathways in the hippocampus of CRND8 transgenic mouse, a model of Alzheimer's disease. Neurosci 2008; 153: 618–33.

32 Ferrer I, Blanco R, Carmona M, Ribera R, Goutan E, Puig B, *et al*. Phosphorylated map kinase (ERK1, ERK2) expression is associated with early tau deposition in neurones and glial cells, but not with increased nuclear DNA vulnerability and cell death, in Alzheimer disease, Pick's disease, progressive supranuclear palsy and corticobasal degeneration. Brain Pathol 2001; 11: 144–58.

33 Dineley KT, Westerman M, Bui D, Bell K, Ashe KH, Sweatt JD. Beta-amyloid activates the mitogen-activated protein kinase cascade via hippocampal alpha7 nicotinic acetylcholine receptors: *In vitro* and *in vivo* mechanisms related to Alzheimer's disease. J Neurosci 2001; 21: 4125–33.

34 Shi C, Zhu X, Wang J, Long D. Intromitochondrial IκB/NF-κB signaling pathway is involved in amyloid β peptide-induced mitochondrial dysfunction. J Bioenerg Biomembr 2014; 46: 371–6.

35 Tsuchiya Y, Asano T, Nakayama K, Kato T Jr, Karin M, Kamata H. Nuclear IKKbeta is an adaptor protein for IkappaBalpha ubiquitination and degradation in UV-induced NF-kappaB activation. Mol Cell 2010; 39: 570–82.

36 Yan J, Xiang J, Lin Y, Ma J, Zhang J, Zhang H, *et al*. Inactivation of BAD by IKK inhibits TNFα-induced apoptosis independently of NF-κB activation. Cell 2013; 152: 304–15.

37 Liu Y, Liu X, Hao W, Decker Y, Schomburg R, Fülöp L, *et al*. IKKβ deficiency in myeloid cells ameliorates Alzheimer's disease-related symptoms and pathology. J Neurosci 2014; 34: 12982–99.

38 Capiralla H, Vingtdeux V, Zhao H, Sankowski R, Al-Abed Y, Davies P, *et al*. Resveratrol mitigates lipopolysaccharide- and Aβ-mediated microglial inflammation by inhibiting the TLR4/NF-κB/STAT signaling cascade. J Neurochem 2012; 120: 461–72.

39 Geetha T, Chen Z, McGregor WC, Douglas White B, Diaz-Meco MT, Moscat J, *et al*. TRAF6 and p62 inhibit amyloid β-induced neuronal death through p75 neurotrophin receptor. Neurochem Int 2012; 61: 1289–93.

40 Tien NT, Karaca I, Tamboli IY, Walter J. Trehalose alters subcellular trafficking and the metabolism of the Alzheimer-associated amyloid precursor protein. J Biol Chem 2016; 291: 10528–40.

41 Poon WW, Carlos AJ, Aguilar BL, Berchtold NC, Kawano CK, Zograbyan V, *et al*. β-Amyloid (Aβ) oligomers impair brain-derived neurotrophic factor retrograde trafficking by down-regulating ubiquitin C-terminal hydrolase, UCH-L1. J Biol Chem 2013; 288: 16937–48.

42 Corsetti V, Florenzano F, Atlante A, Bobba A, Ciotti MT, Natale F, *et al*. NH_2-truncated human tau induces deregulated mitophagy in neurons by aberrant recruitment of Parkin and UCHL-1: implications in Alzheimer's disease. Hum Mol Genet 2015; 24: 3058–81.

43 Guglielmotto M, Monteleone D, Boido M, Piras A, Giliberto L, Borghi R, *et al*. $Aβ_{1-42}$-mediated down-regulation of Uch-L1 is dependent on NF-κB activation and impaired BACE1 lysosomal degradation. Aging Cell 2012; 11: 834–44.

44 Wang Z, Xue Y, Wang P, Zhu J, Ma J. miR-608 inhibits the migration and invasion of glioma stem cells by targeting macrophage migration inhibitory factor. Oncol Rep 2016; 35: 2733–42.

45 Dłużniewska J, Beręsewicz M. Transient cerebral ischemia induces delayed proapoptotic Bad translocation to mitochondria in CA1 sector of hippocampus. Mol Brain Res 2005; 133: 274–80.

46 Fu Z, Yang J, Wei Y, Li J. Effects of piceatannol and pterostilbene against β-amyloid-induced apoptosis on the PI3K/Akt/Bad signaling pathway in PC12 cells. Food Funct 2016; 7: 1014–23.

47 Niino M, Ogata A, Kikuchi S, Tashiro K, Nishihira J. Macrophage migration inhibitory factor in the cerebrospinal fluid of patients with conventional and optic-spinal forms of multiple sclerosis and neuro-Behçet's disease. J Neurol Sci 2000; 179: 127–31.

48 Li Q, Fang J, Yang M, Wu D, Zhang L, Zhang Y. Galantamine inhibits calpain-calcineurin signaling activated by beta-amyloid in human neuroblastoma SH-SY5Y cells. Neurosci Lett 2010; 480: 173–7.

49 Agostinho P, Lopes JP, Velez Z, Oliveira CR. Overactivation of calcineurin induced by amyloid-beta and prion proteins. Neurochem Int 2008; 52: 1226–33.

50 Li SQ, Yu Y, Han JZ, Wang D, Liu J, Qian F, *et al*. Deficiency of macrophage migration inhibitory factor attenuates tau hyperphosphorylation in mouse models of Alzheimer's disease. J Neuroinflammation 2015; 12: 177.

51 Zhang J, Ding YR, Wang R. Inhibition of tissue transglutaminase promotes Aβ-induced apoptosis in SH-SY5Y cells. Acta Pharmacol Sin 2016; 37: 1534–42.

52 Tan X, Li J, Wang X, Chen N, Cai B, Wang G, *et al*. Tanshinone IIA protects against cardiac hypertrophy via inhibiting calcineurin/NFATc3 pathway. Int J Biol Sci 2011; 7: 383–9.

53 Peng XM, Gao L, Huo SX, Liu XM, Yan M. The mechanism of memory enhancement of acteoside (verbascoside) in the senescent mouse model induced by a combination of D-gal and $AlCl_3$. Phytother Res 2015; 29: 1137–44.

54 Yang W, Shi L, Chen L, Zhang B, Ma K, Liu Y, Qian Y. Protective effects of perindopril on d-galactose and aluminum trichloride induced neurotoxicity via the apoptosis of mitochondria-mediated intrinsic pathway in the hippocampus of mice. Brain Res Bull 2014; 109: 46–53.